Numerical study of a well boat operating at a fish farm in long-crested irregular waves and current

Yugao Shen[a,b,*], Marilena Greco[a,b,c], Odd M. Faltinsen[a,b]

[a] *Department of Marine Technology, Norwegian University of Science and Technology (NTNU), Trondheim, NO-7491, Norway*
[b] *Centre for Autonomous Marine Operations and Systems (AMOS), NTNU, Trondheim, NO-7491, Norway*
[c] *CNR-INM, Institute of Marine Engineering, Rome, Italy*

Abstract

The dynamic response of a coupled well boat-fish farm system in irregular long-crested waves and current is analyzed numerically in the time domain. The main purpose is to investigate the influence of the well boat on the fish farm and then to determine the operational conditions of the well boat.

The numerical study of slow-drift sway motion of the well boat is performed at first. Hydrodynamic and statistical theories are briefly introduced. The cross-flow principle is assumed valid for evaluating the transverse viscous loads and the needed cross-sectional drag coefficients are estimated empirically and validated against available experiments. The mean value and standard deviation of the slow-drift motion from time domain agree well with those from frequency domain when equivalent linearized drag damping is incorporated.

The coupled system with the well boat placed at the weather side of the fish farm is then analyzed in detail. Special attention is paid to two critical response variables, i.e., maximum anchor-line loads and maximum floating collar stresses. Numerical results show that the examined two variables will increase more than 300% due to the well boat in moderate exposure sea states. A sensitivity analysis is also carried out to identify the important parameters influencing these two response variables. Cross-sectional drag coefficients for the well boat and fish-farm related parameters (pretension load in the anchor lines and anchor-line stiffness) have moderate influence on the two variables. Simplifying the modeling of the coupled system, for instance neglecting the net cage and the first-order motion, has more effect on the maximum anchor load than on the maximum floating-collar stress and reduced sensitivity is observed in current, especially for the latter variable.

Lastly, the operational conditions of the well boat are determined through systematic simulations. Numerical results show that the maximum loads in the mooring lines are moderate compared with the corresponding breaking limits even in high exposure sea states, while for the maximum stress in the floating collar can be close to the yield stress when operating in moderate exposure regions.

Keywords: Fish farm, Well boat, Irregular waves, Current, Operational conditions

*Corresponding author
Email address: yugao.shen@ntnu.no (Yugao Shen)

1. Introduction

The present work is part of a research study on the dynamic response of a coupled system when a well boat operates at a fish farm during loading/offloading operations. The aim is to investigate the influence of the well boat on the fish farm and in this respect to determine the operational conditions of the well boat for performing such operations. Performing model tests to investigate the problem is challenging due to the issue of Reynolds number scaling. So it is more practical to deal with the problem by numerical simulations.

Shen et al. (2018b) described the background and major motivation for this investigation and presented the numerical results of the response of the coupled system in current only. This study showed that the influence of the well boat is not negligible, in particular, in beam current conditions. For example, the anchor load will increase significantly due to the viscous current loads on the boat. A strong increase of the floating-collar horizontal motions (both rigid and elastic modes) is also expected. In addition, the stress distribution along the floating collar is strongly influenced and the maximum stress occurs at the region where the well boat is in contact with the floating collar and should be of major concern when determining the operational conditions.

It is not sufficient to investigate the coupled system in current only. Irregular waves have to be considered to represent more realistic wave conditions and provide practical guidance. However, to the authors' best knowledge, no attempt of such investigation has been made so far. Shen et al. (2016) performed a numerical study of a coupled well boat-fish farm system in regular waves and current. The idealized fish farm consisted of a flexible-bottomless net cage with sinker weights at the bottom and attached to an elastic circular floater at the top, and was moored with a realistic mooring-line system. The coupling between the ship and the net cage with mooring caused a slowly-varying decaying oscillation with natural period much larger than the considered incident-wave periods. The slowly-varying resonant oscillations can be excited by nonlinear wave loads when the coupled system is exposed to irregular waves and can have an important contribution to the total response of the system.

In this study, numerical modeling of the coupled system in irregular long-crested waves is introduced. The modeling of the fish farm and the coupling between the fish farm and the well boat have been explained in Shen et al. (2018b), so here we will mainly address the modeling of the slow-drift motions of the well boat when the well boat is placed at the weather side of the fish farm, regarded as the most critical scenario. The slow-drift yaw and surge motions are expected to be small in this case, so we will focus on the modeling of the slow-drift sway motion of the well boat. To better explain the modeling and for validation purpose, the fish farm is firstly simplified as a linear spring without damping, then we can model the slow-drift motion by a one-degree-of-freedom equation. Hydrodynamic and statistical theories are provided, e.g., the approach to estimate the slow-drift excitation force and slow-drift damping (wave-drift damping and eddy-making damping) are given. Similar with that shown in Shen et al. (2018b) for estimating the transverse viscous current loads, the transverse viscous loads on the well boat in oscillatory flow only and in combined oscillatory flow and current are estimated by the cross-flow principle documented in Faltinsen (1990) and an empirical approach to

estimate the corresponding cross-sectional drag coefficients is also proposed. The mean value and the standard deviation of the slow-drift motion from the time domain analysis are verified by frequency-domain solutions. Then we proceed to study the coupled system, considering a realistic fish-farm set-up (with single cage). Detailed discussions are given for two critical variables, i.e., maximum anchor loads and maximum floating-collar stresses. A sensitivity analysis is also performed to identify important parameters affecting the examined two variables. The influence of simplifying the modeling of the coupled system is also discussed. In the end, operational conditions of the well boat are determined through systematic simulations. Sea conditions used in the analysis are according to the environmental classification given by Norwegian standard NS9415:2009, see Table 1.

Table 1: Environmental classification given in terms of significant wave height H_s, peak period T_p and current velocity U_∞ according to NS9415 (2009).

Wave	H_s(m)	T_p(s)	**Exposure**	**Current**	U_∞(m/s)	**Exposure**
A	0.0 - 0.5	0.0 - 2.0	Small	a	0.0 - 0.3	Small
B	0.5 - 1.0	1.6 - 3.2	Moderate	b	0.3 - 0.5	Moderate
C	1.0 - 2.0	2.5 - 5.1	Heavy	c	0.5 - 1.0	Heavy
D	2.0 - 3.0	4.0 - 6.7	High	d	1.0 - 1.5	High
E	>3.0	5.3 - 18.0	Extreme	e	>1.5	Extreme

In summary, the present paper is organized as follows. First, a brief description of the numerical set-up of the coupled well boat-fish farm system is given in section 2. Then, numerical modelings of the slow-drift motions of the well boat are introduced in section 3. The corresponding numerical results are shown in section 4. The fish farm is simplified as a linear spring to reduce complexity in the study. Lastly, detailed analysis of the coupled system with a realistic fish-farm set-up is presented in section 5, together with a sensitivity analysis to identify important parameters affecting the maximum anchor loads and floating-collar stresses. The operational conditions of the well boat are also determined through systematic simulations.

2. Numerical set-up

The detailed dimensions of the coupled fish farm-well boat system have been described in Shen et al. (2018b) and will not be shown here to avoid redundancy. The arrangement of the coupled system used in the numerical simulations is reproduced in Figure 1, with the main definitions. The figure also shows the inertial Earth-Fixed reference frames $O_E x_E y_E z_E$ and $O_S x_S y_S z_S$ used in this study. The incident wave angle α_w and current angle α_c are defined in the figure. $\alpha_w = 0^o$ means that the waves propagate in positive x_E direction and $\alpha_c = 0^o$ denotes that the current direction coincides with the positive x_E direction. The heading angle of the boat ψ is also defined in Figure 1 and $\psi = 0^o$ means that the bow of the boat points towards the positive x_E-axis.

For the well boat, a modern design well boat from Rolls-Royce Marine is used in the study. The three-dimensional (3D) numerical panel model used in the potential-flow calculations, together with the lines plan, are shown in Figure 2. The length between perpendiculars is 70 m.

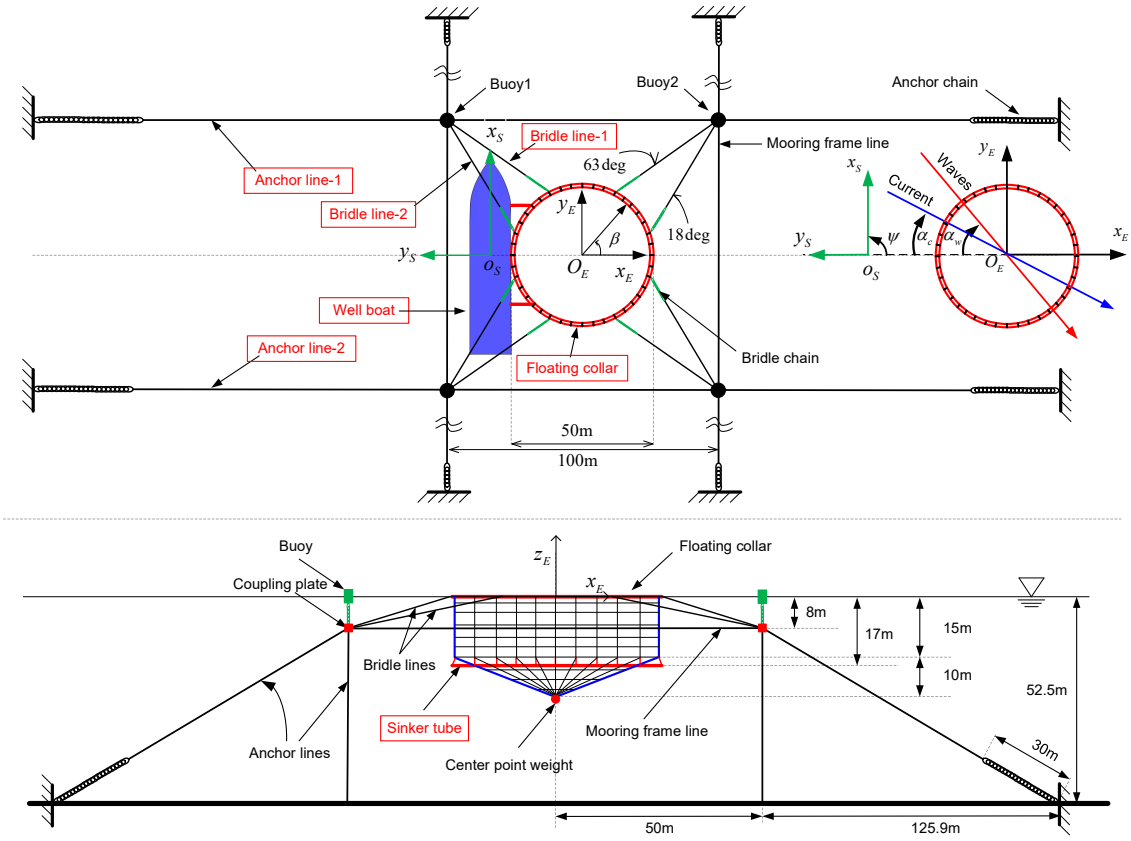

Figure 1: Configurations of the coupled well boat-fish farm system with definitions of the inertial Earth-Fixed coordinate systems $O_E x_E y_E z_E$ and $O_S x_S y_S z_S$ used in this study. Upper: top view. The floating collar is duplicated in the right part of the sketch to define current direction α_c, wave direction α_w and boat heading angle ψ. Lower: side view.

The well boat can be moored in different positions relative to the fish farm. Assuming a scenario with main inflow direction along positive x_E-axis, two different well-boat set-ups are given in Figure 3: one with the well boat at the weather side of the floating collar and the other with the well-boat bow against the inflow. They correspond, respectively, to set-up A and set-up C examined by Shen et al. (2018b) and are named in the same way also here. Based on the studies in current in Shen et al. (2018b), the coupled system with set-up A is expected to be more critical in terms of mooring loads and floating collar stresses and will be our research focus. Results for set-up C will be considered in

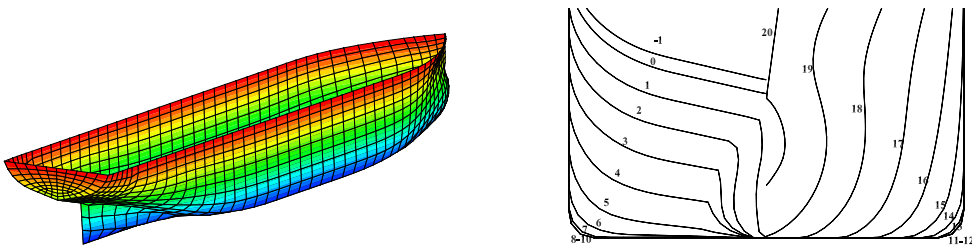

Figure 2: Submerged geometry of the well boat. Left: panel model. Right: body plan. Numbering of sections is also given with section 1 in the aft part of the boat.

selected cases, for comparison.

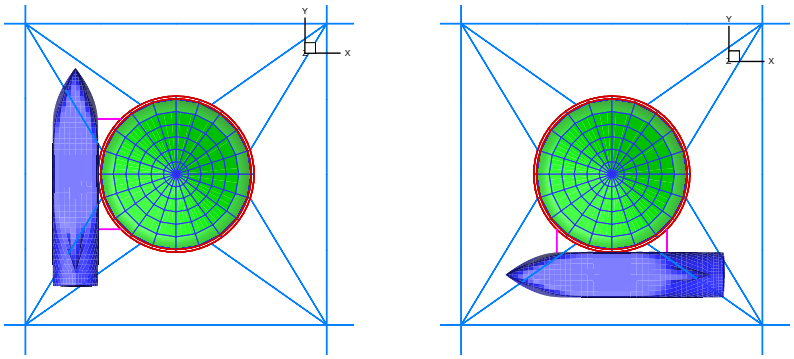

Figure 3: Examined set-ups with the well boat moored to the fish farm from top view. The incident waves and current are in positive x-direction. Left: set-up A, heading angle of the boat $\psi = 90^o$ (weather side). Right: set-up C, $\psi = 180^o$ (bow against waves and current).

3. Theory and numerical model

The modeling of the coupled well boat-fish farm system in current has been documented in Shen et al. (2018b). There, the modelings of the well boat and the different fish-farm components were presented. The strategy used for the well boat-fish farm coupling was also explained. In this section, we will mainly deal with the modeling of the coupled system in irregular waves and current. For the fish-farm system in irregular waves, the numerical modeling was also introduced in Shen et al. (2018b) and is not repeated here. In terms of the well-boat response, apart from the first-order wave-induced motions, the slow-drift resonant oscillations of the well boat may also be excited by non-linear interaction effects between incident waves and body motions. The first-order motions can be solved by the classical seakeeping theory, as shown in Shen et al. (2018b). In this section, we will focus on the slow-drift motions of the well boat.

Irregular long-crested waves and current in positive x_E direction are assumed in the analysis. The modeling of the irregular waves is described in section 3.1. For the coupled system with set-up A (see Figure 3) with the well boat placed at the weather side of the fish farm, the slow-drift surge motion and yaw motion of the well boat are expected to be small and therefore neglected, i.e., only the slow-drift sway motion is considered. To better explain and verify the numerical modeling of the slow-drift sway motion, the fish-farm system is simplified as a linear spring, neglecting the damping due to the net cage and the mooring lines. Then the slow-drift motion can be described by a one-degree-of-freedom equation. Detailed explanation of how to estimate the motion is provided in section 3.2. For the coupled system with set-up C (see Figure 3), the slow-drift sway and yaw motions are expected to be far less important than the slow-drift surge motion, so we will only consider the slow-drift surge motion in the simulations and its modeling is briefly discussed in Section 3.3.

3.1. Irregular waves

The Norwegian standard for design of aquaculture fish farms operating in the sea (NS9415, 2009) requires that the JONSWAP spectrum with $\gamma = 2.5$ for wind-generated seas shall be used for calcu-

lations of response in irregular waves, where γ is the spectral peakedness parameter. As an example, Figure 4 provides the wave spectra for two sea states that will be investigated in sections 4 and 5. They are with $H_s = 2$ m and $T_p = 6$ s, and with $H_s = 1$ m and $T_p = 5$ s, corresponding to moderate exposure and to heavy exposure sea conditions (see Table 1), respectively.

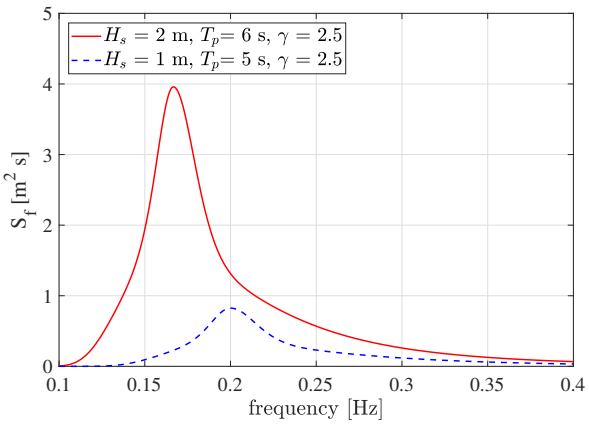

Figure 4: JONSWAP wave spectrum as a function of wave frequency. Solid line: significant wave height H_s=2 m and peak period $T_p = 6$ s. Dashed line: H_s=1 m and $T_p = 5$ s.

The definition of the JONSWAP wave spectrum and detailed procedure to generate the long-crested irregular waves were given in Shen et al. (2018a). Here only the main information on the numerical strategy is provided. In particular, when generating the incident irregular waves, the frequency is evenly distributed into N_f components between $f_{\min} = 0.7/T_p$ and $f_{\max} = 2.0/T_p$ with the length of each interval $\Delta f = (f_{\max} - f_{\min})/N_f$. Here $f_{\min}$ and $f_{\max}$ are the minimum and maximum frequency in Hz of the range where the wave spectrum has energy. The selection of the number of wave components N_f requires some care. We must require that Δf is a small fraction of the smallest natural frequency f_n of the relevant slow-drift response in order to model numerically wave components with frequency sufficiently close to f_n and, therefore, able to excite a resonance condition. In the simulations, $N_f = 500$ is used. Within each frequency interval, a frequency value f_i is randomly selected and, there, the wave spectrum is evaluated, i.e., $S(f_i)$. The random selection of frequencies avoids that the incident-wave time history shows a periodic behavior.

3.2. Coupled well boat-fish farm system with set-up A

In this section, we will focus on the modeling of the coupled system with set-up A. Free decay tests for the coupled system in calm water are performed at first to estimate the natural period and damping of the system. Then, our attention is paid to the modeling of the slow-drift sway motion of the well boat, with a linear spring to represent the fish farm and neglecting the corresponding damping. The governing equation of the motion is introduced, followed by the modelings of the slow-drift excitation force and slow-drift damping. The damping terms may include eddy-making damping and wave-drift damping. Finally, the technique to linearize the eddy-making damping is introduced.

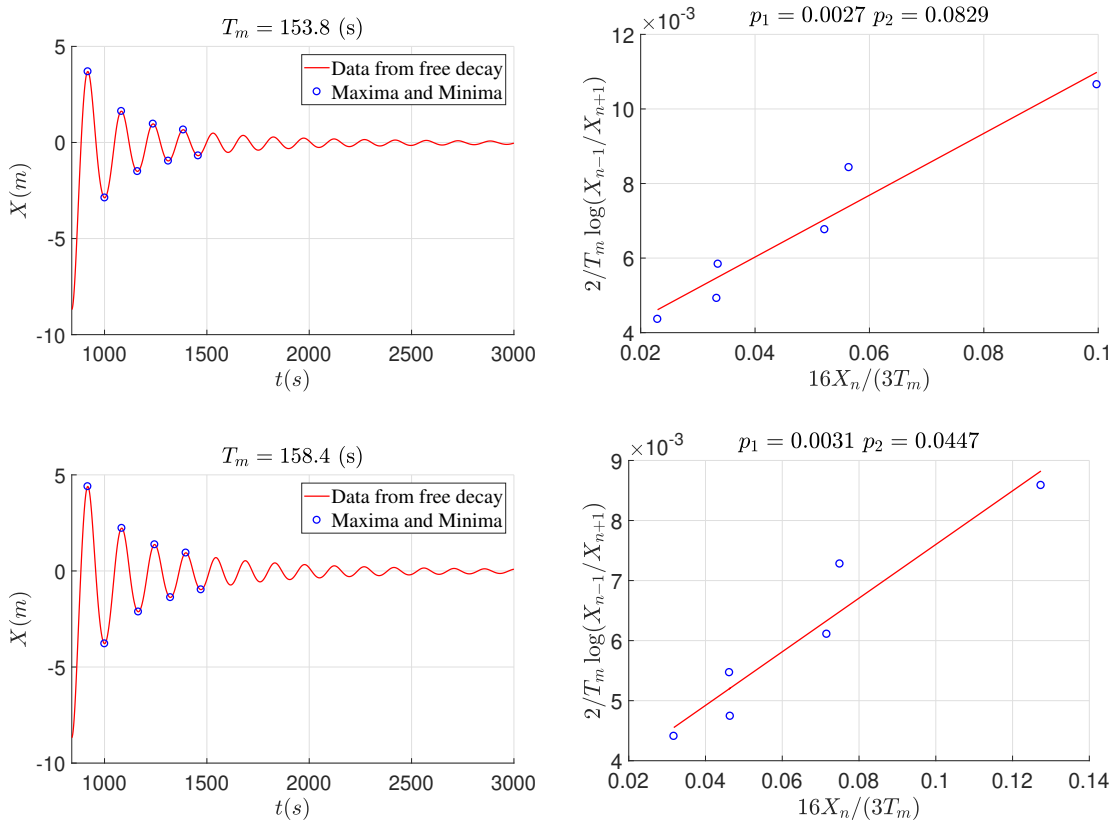

Figure 5: Left: time histories of sway motion of the well boat from free decay tests for the coupled system in calm water. Right: illustration of how to obtain linear damping coefficient p_1 and quadratic damping coefficient p_2 (see e.g., Faltinsen, 1990) . Upper: fish farm with net cage. Lower: fish farm without net cage. X_n is the amplitude of the nth oscillation. T_m is the mean natural period.

3.2.1. Free decay tests

A free decay test for the coupled system in still water is performed to estimate the natural period and the damping coefficients of the system. A ship averaged drag coefficient $C_D = 2.2$ is used for the sway motion of the well boat during the free decay. The reason of using this C_D value can be found in section 3.2.5. The way to estimate the viscous hydrodynamic loads on the fish farm, including the net cage, has been shown in Shen et al. (2018b).

Time history of the sway motion of the well boat during the free decay is shown in the upper row of Figure 5. The linear and quadratic damping coefficients are found according to Faltinsen (1990). The natural period of the coupled system $T_n = 153.8$ s. A free decay test without the net cage is also conducted and the corresponding results are shown in the lower row in Figure 5. The quadratic damping coefficient due to the mooring lines is expected to be small, so the obtained value mainly comes from the well boat. By comparing the drag coefficients from the two cases, we can see that the net cage contributes about 50% to the quadratic damping, but with negligible contribution to the linear damping. It should be noted that the restoring stiffness provided by the fish farm is not constant and also that the quadratic damping coefficient from the net cage is response-amplitude dependent, so the estimated drag coefficient can just serve as a guidance value for the coupled system in oscillatory flow. A free decay test for the coupled system in current is also tried and numerical

result indicates that the system is overdamped.

3.2.2. Well-boat motion equation

To better verify the modeling of the slow-drift sway motion of the well boat, the fish-farm system is simplified and represented by a linear spring. The damping from the fish farm is neglected, as it is not straightforward to be incorporated. In this way, frequency-domain solutions for the slow-drift motion can be obtained. Detailed explanations are given below.

The slow-drift sway motion $\eta_2^{(2)}$ of the well boat in beam-sea irregular waves and collinear current with speed U_∞ can be described by the following one-degree-of-freedom equation

$$\left[M + A_{22}\left(0\right)\right]\ddot{\eta}_2^{(2)} + B_{22}^{SD}\dot{\eta}_2^{(2)} + B_D\left(\dot{\eta}_2^{(2)} - U_\infty\right)\left|\dot{\eta}_2^{(2)} - U_\infty\right| + C_{22}\eta_2^{(2)} = F_2^{SV} \tag{1}$$

where $\ddot{\eta}_2^{(2)} = d^2\eta_2^{(2)}/dt^2$ and $\dot{\eta}_2^{(2)} = d\eta_2^{(2)}/dt$ are the slow-drift acceleration and velocity in sway, M is the mass of the well boat, $A_{22}(0)$ is the zero frequency added mass in sway, B_{22}^{SD} is the wave-drift damping in sway, C_{22} is the equivalent restoring stiffness from the fish farm including the mooring-line and the floating-collar effects and F_2^{SV} is the slow-drift excitation force (including mean value) in sway. B_D is the quadratic damping coefficient connected with the eddy-making damping and can be expressed as $0.5\rho C_D A_Y$ with ρ the water density, A_Y the projected area of the submerged hull in the direction of the sway motion and C_D the corresponding ship averaged drag coefficient. As a first approximation, the influence of the first-order response is neglected when formulating the eddy-making damping. The way to estimate the slow-drift excitation force is documented by, e.g., Faltinsen (1990) and will not be repeated. Here we will focus on the evaluation of the wave-drift damping and the eddy-making damping.

3.2.3. Wave-drift damping

The wave-drift damping for the horizontal motions of a structure is connected with the structure's ability to generate waves and it is a potential flow effect that neglect interaction with flow separation. In fact, this damping is caused by second-order effects in the wave-body interactions and therefore is proportional to the square of the wave amplitude. However it is a linear damping load in terms of the body slowly-varying speed. The presence of the wave-drift damping can be seen by comparing free decay model tests in surge or sway of a large-volume structure in still water and in regular waves. The wave-drift damping in surge or sway can be explained by interpreting the slow-drift surge or sway speed, caused by the wave-body interaction, as a quasi-steady forward and backward speed of the structure (Zhao and Faltinsen, 1988). This "steady" speed can for an observer on the structure be interpreted as an incident steady flow, i.e., a fictitious current with equal and opposite speed, say U_∞. The interaction with the body causes a mean force in the inflow direction that depends on U_∞. For the slowly oscillating body, this force acts as a damping and to a leading order is linearly dependent on U_∞. For example, in case of slowly varying motion in sway, the wave-drift damping coefficient is therefore $B_{22}^{WD} = \frac{\partial \bar{F}_2}{\partial U_\infty}\Big|_{U_\infty=0}$, with $\bar{F}_2$ the mean-wave force in sway direction, and assuming implicitly that the body interacts only with waves, i.e., without a real current. Within this approach, to estimate B_{22}^{WD}, the dependence on U_∞ of the $\bar{F}_2$ experienced by the body must be estimated. In particular,

this can be done by examining the structure in regular waves without current and with current (1) in the same and (2) in opposite direction and then using the approach by Zhao and Faltinsen (1988) to approximate $\frac{\partial \overline{F_2}}{\partial U_\infty}\Big|_{U_\infty=0}$.

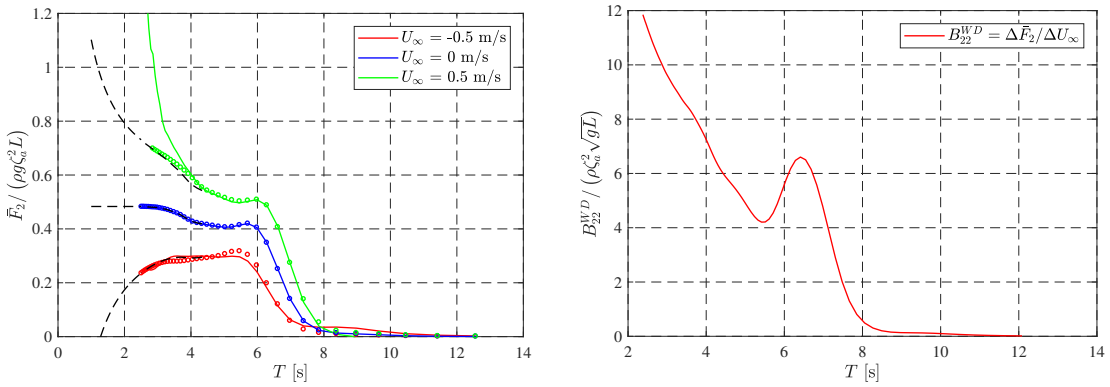

Figure 6: Left: the effect of current on the mean sway force based on potential flow. From the lowest to the highest curve: U_∞=-0.5 m/s to 0.5 m/s. $\bar{F}_2$ is the mean sway force, ξ_a the wave amplitude, ρ the water density, g the gravity acceleration, L the boat length. Solid lines: results from the potential-flow solver HydroStar considering wave-current interactions. Empty circles: results according to formula from Aranha (1994). Dashed lines: results from our simplified analysis by the direct pressure-integration method. Right: wave-drift damping B_{22}^{WD} as a function of wave period T.

Left plot of Figure 6 presents the effect of a current on the mean sway force on the well boat. Regular beam sea waves and three different current velocities are considered with U_∞ = -0.5 m/s, 0 m/s and 0.5 m/s. The positive current is in the wave direction. The potential-flow solver HydroStar (BureauVeritas, 2016) is adopted to estimate the mean-wave loads, considering the wave-current interaction and neglecting the flow separation. The results indicate that, for the well boat in beam sea, a current in the wave direction will significantly increase the mean sway force, especially for cases in short waves. In the HydroStar formulation, only the first-order term in the parameter $\tau = U_\infty \omega_e/g$, being $\omega_e = \omega + kU_\infty$ the encounter frequency with ω the incident wave frequency and $k = \omega^2/g$ the wave number, is kept in the simplified free-surface boundary condition when considering the wave-current interactions. It means that the results in Figure 6 are reliable for small τ. So for very short waves ($T = 2\pi/\omega \leq 4$ s), the results from HydroStar are questionable. In order to characterize the effect of current in high wave frequency, we examined also the results based on the formula proposed by Aranha (1994). This formula is commonly used in engineering practice and there are some disputes about its accuracy. According to Aranha (1994), the mean sway force is influenced by the current velocity as

$$\bar{F}_2(\omega, U_\infty) = \bar{F}_2(\omega_e)(1 + 4U_\infty \omega/g) \tag{2}$$

This expression is formally similar to that given in the short wavelength asymptotic theory by Faltinsen et al. (1980). The results based on eq. (2) are also shown in Figure 6. From the figure, reasonable agreement is observed between them and those from HydroStar for wave period $T \geq 4$ s. We also carried out a simplified analysis by using the direct pressure integration method for cases with very high frequency, i.e., $\omega \to \infty$. It is assumed that the waterline of the well boat near the free surface acts like a vertical wall and that the incoming wave is totally reflected. For the effect of current, only the encounter frequency effect is considered, then we can obtain similar formula as that from Aranha

(1994) and given as

$$\bar{F}_2(\omega, U_\infty) = \bar{F}_2(\omega)(1 + 4U_\infty\omega/g) \tag{3}$$

It should be noted that only the incident wave frequency ω is involved in this formula. Since the applicability of the formula is for very high wave frequency, the difference between ω and ω_e is expected to be small, so the mean wave load predicted, respectively, by eq. (2) and eq. (3) should be similar. The obtained results according to eq. (3) are also shown in the left plot of Figure 6 and indicate a consistency with the formula by Aranha for small values of incident-wave periods. Therefore, the HydroStar's predictions of the mean-drift force in sway have been substituted by the Aranha's formula for T <4 s. The resulting mean-drift force in sway was used to estimate the wave-drift damping presented in non-dimensional form in the right plot of Figure 6.

$B_{22}^{WD}(\omega)/\zeta_a^2$ represents the second-order transfer function of the mean wave-drift damping and can be used to estimate the mean wave-drift damping $\bar{B}_{22}^{SD}$ in irregular long-crested waves as follows

$$\bar{B}_{22}^{SD} = 2\int_0^\infty S(\omega)\left(\frac{B_{22}^{WD}(\omega)}{\zeta_a^2}\right)d\omega \tag{4}$$

Faltinsen and Zhao (1989) argued that there also ought to be a slowly-varying wave-drift damping if there is a slowly-varying excitation force and it can be expressed in a similar way as the slow-drift excitation force. Detailed expression can be found in Faltinsen and Zhao (1989) and is not given here.

3.2.4. Eddy-making damping

Eddy-making damping is usually also important for the estimation of slow-drift sway motion. Here, this is calculated by strip theory assuming valid the cross-flow principle. In order to have a reliable prediction of its value, we need a reliable estimation of the drag coefficient at the different ship cross-sections. Detailed procedures to estimate the cross-sectional drag coefficients for cases in oscillatory flow only and in combined oscillatory flow and current are demonstrated, respectively, in section 3.2.5 and section 3.2.6. The oscillatory flow is mono-chromatic and associated with the natural sway period. The 3D flow effects are also accounted for and estimated by using a reduction factor in a similar way as was done in estimating transverse current forces in Shen et al. (2018b).

3.2.5. Cross-sectional drag coefficient in oscillatory flow

Faltinsen (1990) showed that the cross-flow drag coefficient for ship cross-sections in mono-chromatic oscillatory flow depends on the section geometry (beam-to-draft ratio, bilge radius, bilge keel presence and dimensions), the Keulegan-Carpenter number $KC = U_M T/D$ (with U_M = amplitude of oscillatory relative velocity between the body and the ambient flow, T = oscillatory period, D = sectional draft), the free-surface and three-dimensional (3D) effects. A brief explanation of the different parameters will be given in the following.

Free surface: For the slow-drift oscillation in sway, relevant characteristic KC number is expected to be less than 10. Then the free surface will have little influence on the drag coefficient, according to Faltinsen (1990).

Cross-sectional shape: The effect of the cross-sectional shape on the drag coefficient for typical midship sections is mainly due to the bilge radius r, beam-to-draft ratio B/D and bilge keels. Increasing the bilge radius means decreasing the drag coefficient. The beam-to-draft ratio will have influence, but only when $B/(2D) < 1$. In terms of the bilge keels, the drag coefficient depends strongly on the bilge-keel breadth.

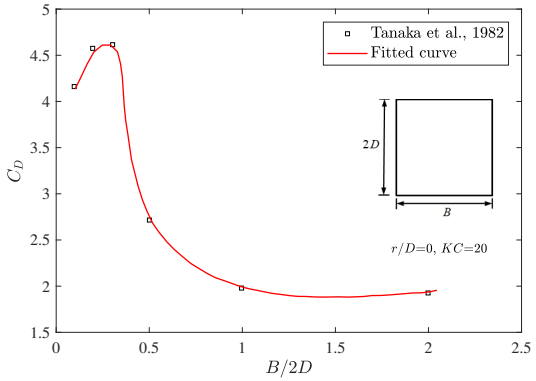

Figure 7: Drag coefficient C_D as a function of aspect ratio $B/2D$ for a rectangular cylinder with sharp corners at KC =20 (Tanaka et al., 1982).

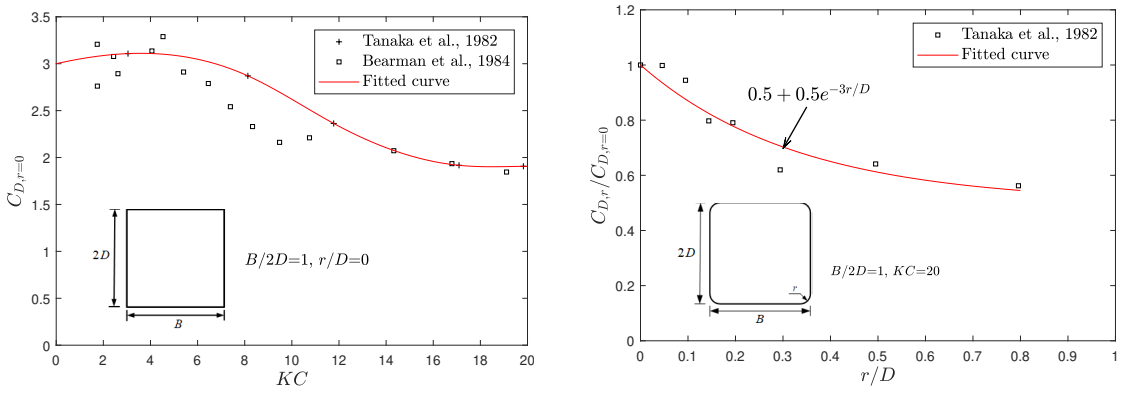

Figure 8: Left: drag coefficient C_D as a function of KC for a sharp-edged square cylinder from Tanaka et al. (1982) and Bearman et al. (1984). Right: drag coefficient C_D as a function of r/D at KC=20. Experimental results are from Tanaka et al. (1982). The fitted curves are used in the analysis.

For a rectangular cross-section, the drag coefficient will be obtained by adjusting the value for a sharp-edged square cross-section, considering the influence of aspect ratio and bilge radius. The reason is that relevant information of the drag coefficient for a square cross-section is more readily available. Detailed procedure used here is explained below. The dependence of the drag coefficient C_D on the aspect ratio $B/(2D)$ for a sharp-edged rectangular cross-section at $KC = 20$ is shown in Figure 7 (see Tanaka et al., 1982). The dependence is assumed to be applicable also for $KC < 20$. If the drag coefficient for a square section is known, then the value for a general rectangular section can be obtained, considering the aspect ratio influence. So our main attention is paid to the estimation of C_D for a square section. The drag coefficient $C_{D,r=0}$ for a sharp-edged square section as a function of KC number is shown in the left plot of Figure 8 (see Tanaka et al., 1982 and Bearman et al., 1984). A fitted curve of the experimental data is also provided in the figure and will be used in the analysis.

On the other hand, experimental results by Tanaka et al. (1982) show that there is a strong effect of the bilge radius on the drag coefficient, see the right plot of Figure 8. Similarly as done by Shen et al. (2018b) for a section in steady flow, a best fit of these experimental data is estimated, giving $C_{D,r}/C_{D,r=0}|_{KC=20} = 0.5 + 0.5e^{-3r/D}$. The examined KC is 20, but the bilge-radius influence on the C_D is assumed applicable also for $KC < 20$, as we do not have any other experiments for another KC lower than 20. This is an error source in the numerical results. This means that $C_{D,r}$ for a given KC can be evaluated by $C_{D,r} = C_{D,r=0}(0.5 + 0.5e^{-3r/D})$, with $C_{D,r=0}$ given by the fitted curve in the left plot of Figure 8 as a function of KC number. Once $C_{D,r}$ for a square section is obtained, by accounting for the influence of aspect ratio $B/(2D)$, the drag coefficient $C_{D,r}$ for a generic rectangular section at different KC numbers can be estimated.

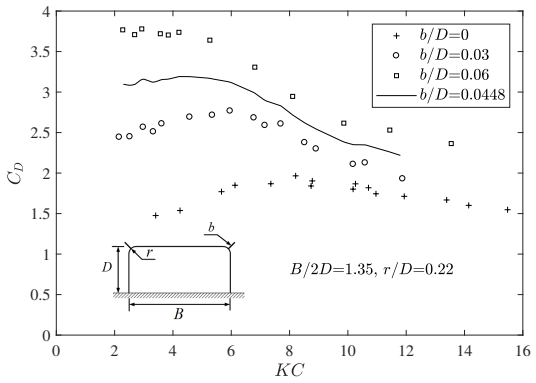

Figure 9: The effect of bilge keels on the drag coefficient C_D at small KC numbers. Symbols: experimental data from Faltinsen and Sortland (1987). Solid curve: interpolated value for the cross-section of the well boat equipped with bilge keels.

Next, we will show how the drag coefficients for different cross-sections of the well boat are predicted. For the ship sections without bilge keels and with geometry close to a rectangle (sections 4-6, 14-18, see Figure 2), the same procedure as the one described for a rectangular cross-section has been followed. For sections with bilge keels (sections 7-13), the above introduced procedure cannot be applied, as the drag coefficient depends strongly on the breadth of the bilge keels. Instead, we estimate the drag coefficient based on the experimental data from Faltinsen and Sortland (1987). In these experiments, $B/(2D) = 1.35$, $r/D = 0.22$ and three bilge-keel breadth-to-draft ratio $b/D = 0$, 0.03 and 0.06 were examined. In our case, for the considered well-boat sections, $B/(2D) = 1.12$, $r/D = 0.15 - 0.23$ and $b/D = 0.0448$. The drag coefficient is expected to be mainly determined by the parameter b/D, so its value can be obtained through interpolating the experimental data in terms of b/D, see Figure 9. There are differences of $B/(2D)$ and r/D between the well-boat sections with bilge keels and the sections studied experimentally and given in the figure, but their effect is expected to be small, based on the results shown in Figures 7 and 8.

The well-boat sections near the ship ends (section 1-3, 19-20, see Figure 2) present shapes not studied experimentally or numerically. A rough estimation of their drag coefficients has been obtained by assuming that the flow around one of these cross-sections resembles that around a flat plate and $C_D = 8.0\ KC^{-1/3}$ is assumed for small KC, as documented in Faltinsen (1990). This is an error

source but has a limited influence on the average drag coefficient for the well boat, as explained in Shen et al. (2018b). Similarly as shown by Shen et al. (2018b) in steady flow, the 2D drag coefficient for different sections needs to be lowered as consequence of three-dimensional (3D) effects and the same reduction factor as the one for steady flow is adopted here because no study on 3D effects for oscillatory flow is available in literature.

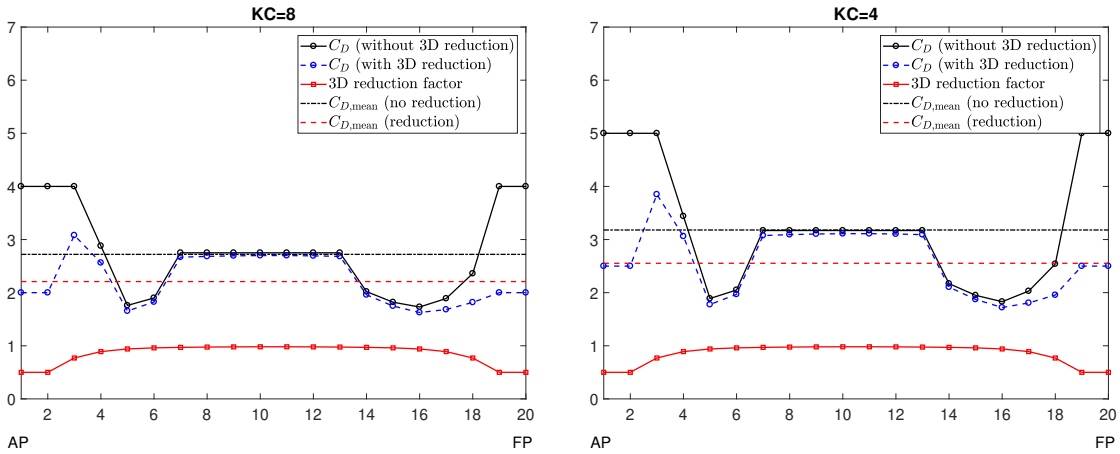

Figure 10: Sectional transverse drag coefficient $C_D(x)$ for different sections of the examined well boat. Left: KC=8. Right: KC=4. The 2D drag coefficients with and without the 3D reduction effects are shown. The corresponding ship averaged drag coefficients are also given.

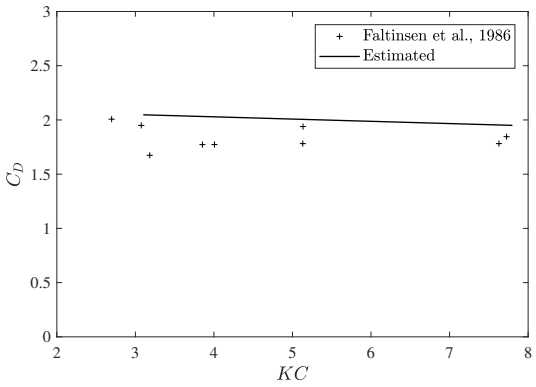

Figure 11: Drag coefficient for slow-drift sway motion of the well boat as a function of KC number. Symbols: experimental data from Faltinsen et al. (1986). Solid line: drag coefficient estimated with the empirical approach proposed here.

Figure 10 shows the estimated drag coefficients for different sections of the well boat at KC=8 (left plot) and KC=4 (right plot). From the figure, the ship averaged drag coefficients are about 2.2 and 2.5 for KC=8 and KC=4, respectively, which indicates that the average drag coefficient is not so sensitive to the change of KC number, in the KC range relevant for our application. In order to assess the method proposed here, we applied it to estimate the average transverse drag coefficient for a ship for which experimental data are available in Faltinsen et al. (1986). The results are shown in Figure 11. From them, the empirically estimated average drag coefficients agree well with the experimental data at different KC numbers. This suggests a fair reliability of the approach proposed for the C_D prediction in oscillatory flow.

3.2.6. Cross-sectional drag coefficient in combined oscillatory flow and current

Current may have an important effect on the eddy-making damping and its influence on wave-drift damping and slow-drift excitation force should also be considered. Sarpkaya and Storm (1985) conducted experiments with circular cylinders moving with constant velocity in a sinusoidally oscillating flow to determine the drag and inertial coefficients and found that, in general, the drag and inertia coefficients obtained for coexisting waves and current (both when following the waves and when in opposite direction) were found to be much smaller than the drag and inertia coefficients derived in waves alone for small KC number. They pointed out that the force coefficients were governed by Keulegan-Carpenter number $KC = U_M T/D$, Reynolds number $Re = U_M D/\nu$, alternatively expressed by their ratio $Re/KC = \beta = D^2/\nu T$, and by the reduced velocity $VK = U_\infty T/D$. Here the involved parameters are defined as above in this section and ν is the kinematic viscosity coefficient of water. Hamel-Derouich (1993) carried out experiments for smooth sharp-edged rectangular cylinders. The cylinders were horizontally submerged and tested in wavy flow and in combined steady and wavy flows, corresponding to low KC numbers up to a value of 8. Three different reduced velocities were considered, i.e., VK=8, 12, 16. The experiments showed that the drag coefficient measured in conditions without current overestimated the measured wave-current induced non-dimensional forces and the drag coefficient under combined waves and current was quite close to the value in steady flow and was less KC-number dependent, especially for larger reduced velocity. The phenomenon can be explained by the fact that when $U_c/U_M > 1$, the returning vorticity due to the oscillatory part of the flow has a small influence on the inflow velocity to the body, so the influence of KC on C_D is small. In the present analysis, $U_c/U_M \geq 1$ for the cases relevant for determining the operational conditions of the well boat. Therefore, the drag coefficient for steady flow will be adopted for cases with waves and current. A sensitivity analysis will be performed to investigate the influence of the variation of the drag coefficient.

3.2.7. Slow-drift sway response

If only the mean value and the standard deviation of the sway response are targeted, the time-varying feature of the wave-drift damping can be neglected (see e.g., Faltinsen, 1990). It means that only the mean wave-drift damping, as discussed in section 3.2.3, can be considered, i.e., $B_{22}^{SD} \approx \bar{B}_{22}^{SD}$. If then the nonlinear eddy-making damping is approximated with an equivalent linear damping, eq. (1) can be solved in the frequency domain. Relative to a time-domain solution, this is a very robust and time-efficient way to obtain the mean value and standard deviation of the motion. In particular, the nonlinear eddy-making damping term is linearized through an equivalent stochastic linearization, see Price and Bishop (1974) and Roberts and Spanos (2003). By assuming a Gaussian response, which is not strictly true, we can obtain an equivalent linear damping coefficient, in the form

$$B_{22}^{e} = B_D \left[\frac{4}{\sqrt{2\pi}} \sigma_{\dot{\eta}_2^{(2)}} \exp\left(-0.5 U_\infty^2 / \sigma_{\dot{\eta}_2^{(2)}}^2\right) + 2 U_\infty \Phi\left(\frac{U_\infty}{\sqrt{2}\sigma_{\dot{\eta}_2^{(2)}}}\right)\right] \tag{5}$$

where Φ is the error function whose detailed expression can be found in any standard mathematical handbook (see e.g., Abramowitz and Stegun, 1965), $\sigma_{\dot{\eta}_2^{(2)}}$ is the standard deviation of the slow-drift

sway velocity. We can approximate $\sigma_{\dot{\eta}_2^{(2)}}$ as $\mu_n \sigma_{\eta_2^{(2)}}$, where $\sigma_{\eta_2^{(2)}}$ is the standard deviation of slow-drift sway motion and $\mu_n = \sqrt{C_{22}/\left[M + A_{22}\left(0\right)\right]}$ is the natural undamped circular frequency in sway. For zero current velocity, i.e., $U_\infty = 0$ m/s, $B_{22}^e = 4B_D\sigma_{\dot{\eta}_2^{(2)}}/\sqrt{2\pi}$. This is consistent with the expression documented in Faltinsen (1990). Eq. (1) can then be written as

$$\left[M + A_{22}\left(0\right)\right]\ddot{\eta}_2^{(2)} + B_{22}\dot{\eta}_2^{(2)} + C_{22}\eta_2^{(2)} = F_2^{SV} \tag{6}$$

with $B_{22} = \left(\bar{B}_{22}^{SD} + B_{22}^e\right)$ the sum of mean wave-drift and linearized eddy-making damping coefficients. The mean square value of $\eta_2^{(2)}$ can be written as (see e.g., Faltinsen, 1990)

$$\sigma_{\eta_2^{(2)}}^2 = \int_0^\infty \frac{S_F\left(\mu\right)d\mu}{\left\{C_{22} - \left[M + A_{22}\left(0\right)\right]\mu^2\right\}^2 + B_{22}^2\mu^2} \tag{7}$$

Here S_F is the spectral density for the slow-drift excitation force, B_{22} is also a function of $\sigma_{\eta_2^{(2)}}$, so there are the unknown $\sigma_{\eta_2^{(2)}}$ on both the left- and right-hand side of eq. (7) and iteration is needed to obtain $\sigma_{\eta_2^{(2)}}$.

3.3. Coupled well boat-fish farm system with set-up C

In set-up C, the slow-drift surge motion of the well boat is excited and needs to be estimated. For this, the same procedure as the one shown in section 3.2 for estimating the slow-drift sway motion is followed. To avoid redundancy, here we just outline the approach to find the slow-drift damping in surge, including wave-drift damping and viscous hull damping.

3.3.1. Wave-drift damping

Left plot of Figure 12 shows the effect of current on the mean wave force in surge for the well boat. Different from the beam-sea condition (see Figure 6), the current presence will have a small influence on the mean surge force in shorter waves (wave period $T \leq 6s$). For very short waves ($T \leq 4s$), the results from HydroStar are not reliable, as explained in section 3.2.3. Aranha's formula is also employed to account for the current influence (not shown here), but poor agreement is observed compared with the results from HydroStar. This indicates that such formula is applicable for beam-sea waves and current, but not for head-sea scenario. Results from short wavelength asymptotic theory by Faltinsen et al. (1980) are also given and are used to estimate the wave-drift damping for shorter waves, to overcome the limitations of the HydroStar predictions in this wave-frequency range. The requirement by the asymptotic theory that the ship hull surface at the mean waterline should be vertical is not exactly satisfied by the examined well boat and is regarded as an error source. The wave-drift damping for slow-drift surge motion obtained with this approach is shown in the right plot of Figure 12 as a function of the wave period. From the figure, the wave-drift damping is small especially for shorter waves ($T \leq 6$ s). This suggests that, for the sea states relevant in our analysis (peak period $T_p \leq 6s$), the wave-drift damping is expected to be not so important.

3.3.2. Viscous damping

The prediction of the viscous surge force on the well boat in non-separated oscillatory flow is addressed here. The boundary-layer flow can be turbulent or laminar depending on the characteristic

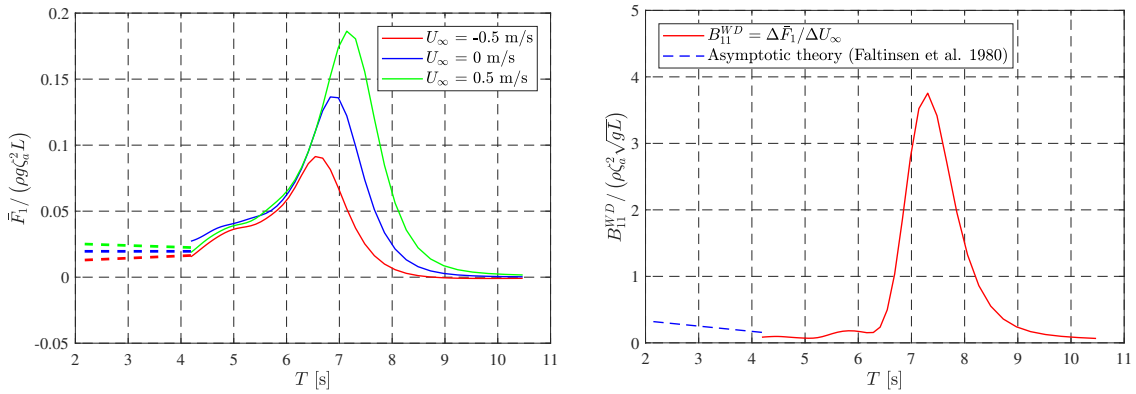

Figure 12: Left: the effect of current on the mean surge force. From the lowest to the highest curve: U_∞=-0.5 m/s to 0.5 m/s. $\bar{F}_1$ is the mean surge force. Solid lines: results from the potential-flow solver HydroStar considering wave-current interactions. Dashed lines: results from short-wavelength asymptotic theory (Faltinsen et al., 1980). Right: wave-drift damping in surge B_{11}^{WD} for the well boat as function of the wave period T. The solid line indicates the part predicted with HydroStar and the dashed line the part predicted with the short-wavelength asymptotic theory.

Reynolds number. The flow is likely to be turbulent in full scale. Jonsson (1980) proposed empirical formulas for the shear stress that apply to turbulent flow along fixed-plane surfaces. Outside the boundary layer, the flow oscillates harmonically. Jonsson defines the Reynolds number as

$$RE = U_M^2/\omega\nu = \omega A_0^2/\nu \tag{8}$$

where ω is the oscillatory circular frequency and A_0 the oscillatory amplitude. For the slow-drift surge motion, ω and A_0 are taken, respectively, as the resonance frequency and the standard deviation of the motion. $RE = 10^5$ is proposed as an engineering criterion for transition to turbulent boundary-layer flow for a smooth surface. When the surface is smooth, Jonsson writes the maximum wall shear stress τ_{wm} as

$$2\tau_{wm}/\frac{1}{2}\rho U_M^2 = 0.09RE^{-0.2} \tag{9}$$

However, when considering the viscous force in surge on the well boat connected with the non-separated turbulent boundary-layer flow, it is not sufficient to account for the shear stresses. Since the ship surface has a finite curvature, it follows that there is an in/out flow through the boundary layer (Faltinsen and Timokha, 2009). The in/out flow is associated with pressure gradient. It means that there is also a pressure drag force. We write the total drag force in the longitudinal ship direction as

$$F_{D,x} = \frac{1}{2}\rho\left(0.09RE^{-0.2}S_w + C_pA_X\right)\dot{\eta}_1^{(2)}\left|\dot{\eta}_1^{(2)}\right| = C_X\dot{\eta}_1^{(2)}\left|\dot{\eta}_1^{(2)}\right| \tag{10}$$

Here S_w is the mean wetted-surface area, C_p and A_X are the drag coefficient and the mean-wetted projected area in the longitudinal ship plane, C_X is the corresponding total viscous force coefficient, $\dot{\eta}_1^{(2)}$ is the slow-drift velocity in surge. Projected area A_X can be approximated as $B \times D$. By applying eq. (10) to the ship presented in Faltinsen et al. (1986) and comparing with their experimentally obtained C_X from free-decay test, we have $C_p = 0.59$ for their ship, once substituted in the C_X expression of eq. (10) the values for RE, S_w and A_X. Since the geometry of the ship examined by

Faltinsen et al. (1986) is quite close to the present well boat, the same C_p will be used for the well boat.

4. Slow-drift response of the well boat

In this section, we present numerical results of the slow-drift sway motion of the well boat, described by the one-degree-of-freedom motion equation in section 3.2. The main purpose is to verify the modeling of the slow-drift motion and investigate the influence of different parameters on the motion. This will serve as a guidance for the study of the coupled well boat-fish farm system in section 5. In the following analysis, this coupling is simplified and the load on the well boat due to the fish-farm system is simplified as a linear spring. A stiffness $C_{22} = 24$ kN/m is assumed, corresponding to the restoring stiffness provided by the fish farm when there is no anchor chain laying on the seabed (Shen et al., 2018b).

4.1. Slow-drift sway motion

The slow-drift motion is estimated here by solving in time eq. (1). The importance of different slow-drift damping terms is discussed and the necessity of considering the first-order motion when calculating the eddy-making damping is also studied. In addition, different statistic approaches are used to examine the extreme values obtained from time-domain simulations with different time durations.

4.1.1. Wave-drift damping

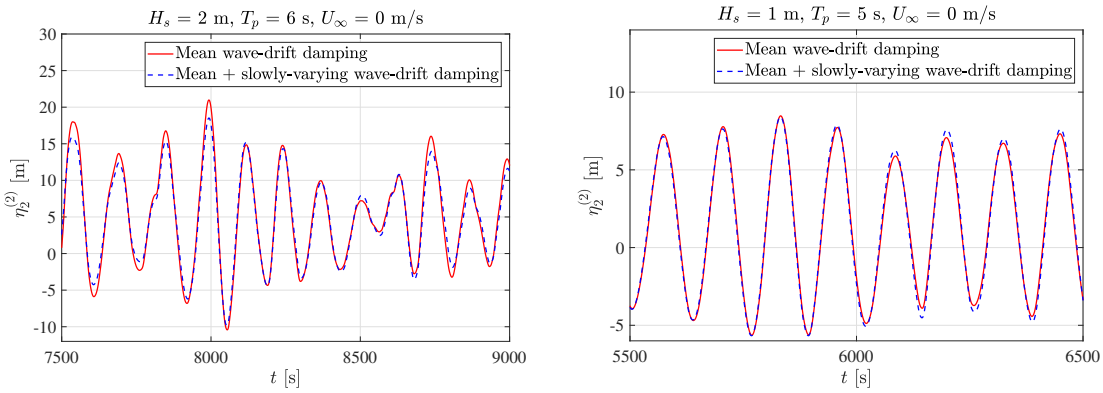

Figure 13: Time histories of the slow-drift motion in sway. Just a short time interval when the motion reaches the largest maximum in the performed simulation is shown. The duration of the simulations is 3 hours. Solid line: numerical solution of eq. (1) with mean wave-drift damping. Dashed line: numerical solution of eq. (1) with mean plus slowly-varying wave-drift damping. Left: $H_s = 2$ m and $T_p = 6$ s. Right: $H_s = 1$ m and $T_p = 5$ s.

Figure 13 shows the time histories of the slow-drift sway motion of the well boat, considering in eq. (1) the mean wave-drift damping and the mean plus slowly-varying wave-drift damping, respectively. The eddy-making damping is not included. Two wave conditions with $H_s = 2$ m, $T_p = 6$ s and with $H_s = 1$ m, $T_p = 5$ s, respectively, are considered. The figure shows that considering the slowly-varying wave-drift damping will reduce the maximum motion for $H_s = 2$ m and $T_p = 6$ s, while negligible influence is observed for $H_s = 1$ m and $T_p = 5$ s. Detailed analysis is given below.

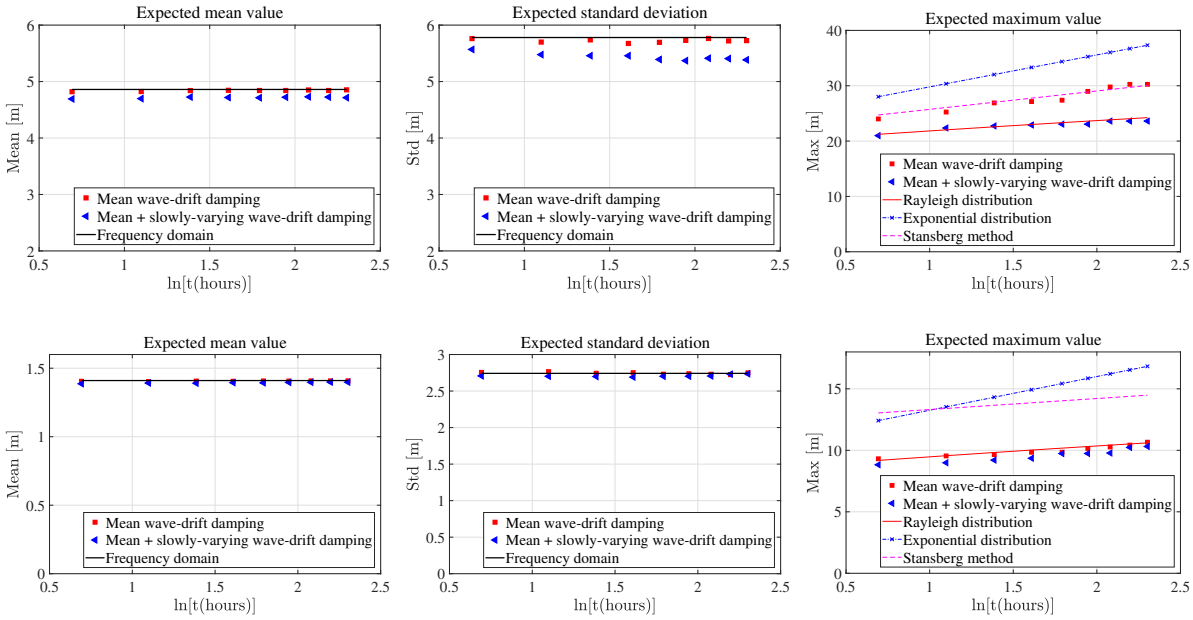

Figure 14: Expected mean value (left), standard deviation (middle) and maximum value (right) of the slow-drift sway motion. Only the wave-drift damping is included. Upper: $H_s = 2$ m, $T_p = 6$ s, $U_\infty = 0$ m/s. Lower: $H_s = 1$ m, $T_p = 5$ s, $U_\infty = 0$ m/s. The predicted maximum values based on Rayleigh distribution (including only the mean wave-drift damping), exponential distribution and Stansberg's method (including only the mean wave-drift damping, see Stansberg, 1991) are also shown.

- Irregular waves with $H_s = 2$ m, $T_p = 6$ s:

  The expected mean value $\bar{\eta}_2^{(2)}$, the standard deviation $\sigma_{\eta_2^{(2)}}$ and the maximum value $\eta_{2,\max}^{(2)}$ of the slow-drift motion from time-domain simulations are presented in the upper row of Figure 14 as a function of simulated time (from 2 hours up to 10 hours). Ten different realizations are considered and the simulated time of each realization is 10 hours. In the analysis, portions of each realization are considered, with duration varying from 2 hours to 10 hours, and treated as individual realizations to see the effect of the simulated time. Each value in the figure is taken as the mean value from ten different realizations. From the figure, the expected mean value and standard deviation are almost independent from the simulated time. Including the slowly-varying wave-drift damping will reduce the mean value, the standard deviation and the maximum value, with the maximum value the most affected. The frequency-domain solutions of the standard deviation from eq. (7) and the mean sway motions caused by the mean wave loads are also provided. In this case the slowly-varying wave-drift damping cannot be accounted for. The figure shows that the expected mean value and the standard deviation from the time-domain analysis agree nicely with those from the frequency-domain solution. The mean value and the standard deviation from frequency domain are 4.86 m and 5.78 m, respectively. In terms of the damping level, the considered mean wave-drift damping is $\xi = 7.86\%$ of the critical damping.

- Irregular waves with $H_s = 1$ m, $T_p = 5$ s:

  The expected mean value, the standard deviation and the maximum value of the slow-drift motion

are presented in the lower row of Figure 14. Also in this case nice agreement is observed for the mean value and the standard deviation between the time-domain and the frequency-domain results. The mean value and the standard deviation from frequency domain are 1.41 m and 2.74 m, respectively. The mean wave-drift damping is $\xi = 2.22\%$ of the critical damping. Including the slowly-varying wave-drift damping has negligible influence on the motion due to the small damping level.

Three different statistical approaches are used to examine the expected largest sway motion from the time-domain simulations. One is based on the use of the Rayleigh distribution. This is theoretically sound when the damping is linear, time-independent and asymptotically small. So only the mean wave-drift damping can be included. The expected largest value $\eta^{(2)}_{2,\max}$ can then be written as

$$\eta^{(2)}_{2,\max}(t_s) \approx \sigma_{\eta^{(2)}_2}\sqrt{2\ln N} + \bar{\eta}^{(2)}_2 \tag{11}$$

where t_s is the simulated time, N is the number of slow-drift oscillations during t_s. This can be estimated as $N = t_s/T_n$ with T_n the natural period of the slow-drift motion. The standard deviation $\sigma_{\eta^{(2)}_2}$ can be obtained from frequency-domain or time-domain analysis.

The second approach is to use exponential distribution as a rough approximation to estimate the extreme slow-drift response. This was suggested by Naess (1989). In this case, the expected maximum value takes the form

$$\eta^{(2)}_{2,\max}(t_s) = \sigma_{\eta^{(2)}_2}\ln N + \bar{\eta}^{(2)}_2 \tag{12}$$

Eq. (12) is generally on the conservative side and the smaller is the damping the more it is conservative.

The third approach is based on a simple statistical model proposed by Stansberg (1991). A critical point in the use of such model is the determination of the relative spectral bandwidth parameter, defined as the ratio between the width of the wave group spectrum and the width of the slow-drift response spectrum. Detailed formulas will not be shown here. More accurate estimation procedure is possible (Naess, 1986), but the quadratic transfer function (QTF) of the wave-drift force on the well boat must be known and the estimation of this is not attempted in the present work.

Detailed comparison of the expected largest values obtained directly from the time-domain simulations and using the three theoretical statistical approaches for the considered two sea states are shown in the right of Figure 14. From the figure, the exponential distribution clearly overestimates the extreme values for both cases. The Rayleigh distribution can well-predict the extreme values for $H_s = 1$ m and $T_p = 5$ s, when the damping is small, but will underpredict the extreme values for $H_s = 2$ m and $T_p = 6$ s associated with relatively large damping ($>$ 3-4% of the critical damping). The Stansberg's method has a nice prediction of the extreme values for cases with $H_s = 2$ m and $T_p = 6$ s but overpredicts the results for cases with $H_s = 1$ m and $T_p = 5$ s.

Figure 15 presents the standard deviation and maximum value of the slow-drift motion from ten different realizations (same as those shown in Figure 14) with $H_s = 2$ m and $T_p = 6$ s. The first 3-hour simulation of each realization is considered. The figure shows that both the standard deviation and the maximum value are realization dependent. At least 10-20 realizations are needed to have a robust estimation of the two examined variables.

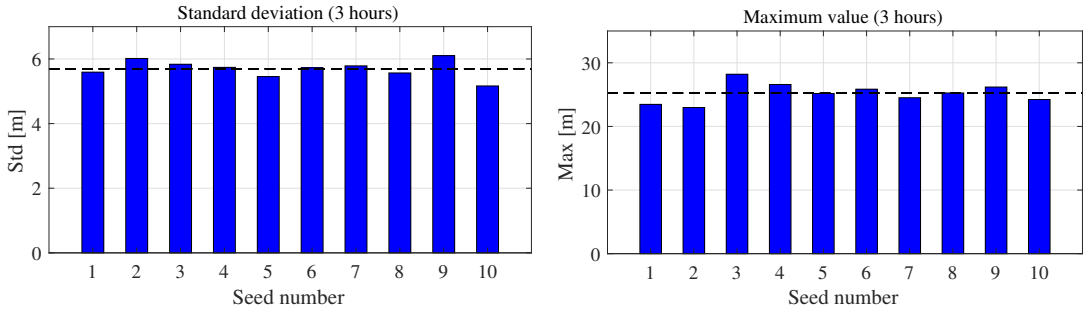

Figure 15: Standard deviation (left) and maximum value (right) of the slow-drift sway motion from different realizations with only mean wave-drift damping considered. The considered $H_s = 2$ m, $T_p = 6$ s, $U_\infty = 0$ m/s. The numbering along the horizontal axis represents the use of different random-phase seeds to generate the incident irregular waves. In each plot, the dashed line represents the expected value, taken as the mean value from different realizations.

4.1.2. Eddy-making damping

In this section, the analysis of the slow-drift sway motion is carried out assuming that the slow-drift damping is only associated with the eddy-making damping. Figure 16 presents the influence of the ship averaged drag coefficient on the expected standard deviation and on the largest value of the slow-drift motion in irregular waves. Two different wave conditions are considered with $H_s = 2$ m, $T_p = 6$ s (upper row) and with $H_s = 1$ m, $T_p = 5$ s (lower row), respectively. Two different ship averaged drag coefficients $C_D = 2.2$ and 0.9 are examined, corresponding to the value for oscillatory flow (KC =8) and for steady flow, respectively. The main purpose to use two different C_D is to examine the sensitivity of the slow-drift motion to C_D. Detailed explanations are given below.

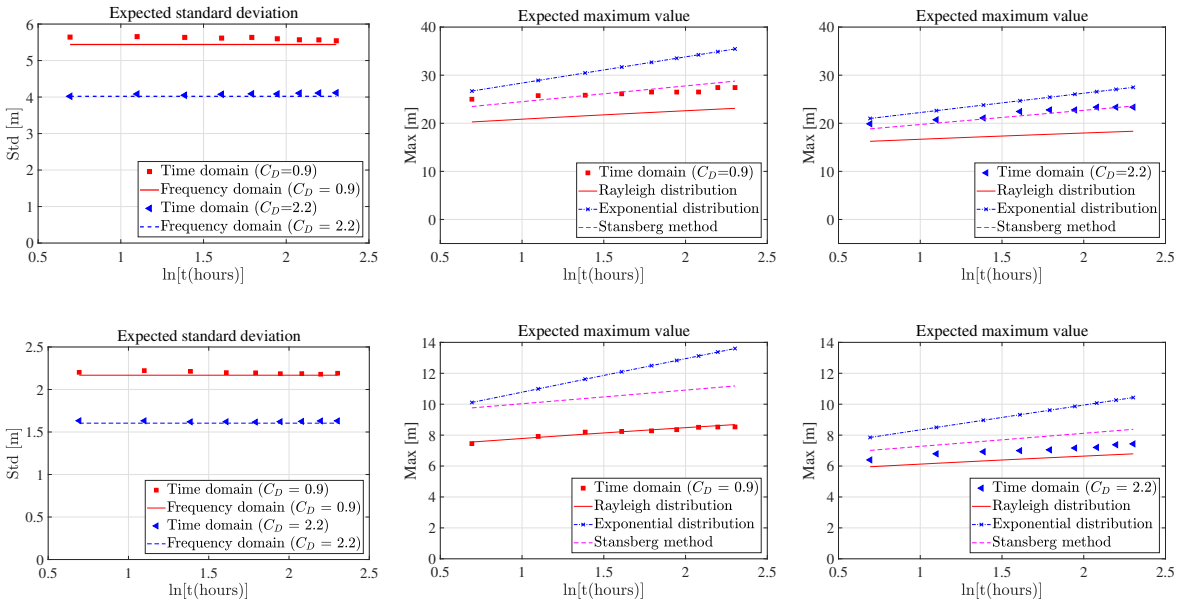

Figure 16: Expected standard deviation (left) and maximum value (middle with $C_D = 0.9$ and right with C_D= 2.2) of the slow-drift sway motion. Only the eddy-making damping is included. Full symbols: time-domain results. Upper: $H_s = 2$ m, $T_p = 6$ s, $U_\infty = 0$ m/s. Lower: $H_s = 1$ m, $T_p = 5$ s, $U_\infty = 0$ m/s. The expected maximum values predicted by Rayleigh distribution, exponential distribution and Stansberg's method are also provided.

- Irregular waves with $H_s = 2$ m, $T_p = 6$ s:

The expected standard deviations obtained from both time-domain and frequency-domain solutions are provided and agree for the two C_D values, see the left plot in Figure 16. The eddy-making damping is linearized according to eq. (5) in the frequency-domain solution. The ratio between the linearized damping and the critical damping is $\xi = 16.2\%$ and 8.89%, respectively, when $C_D = 2.2$ and 0.9 are used. For 3-hour simulated time, the expected standard deviations are 4.08 m and 5.65 m, respectively, for the two values of the C_D, indicating approximatively a dependence on C_D as $C_D^{-1/3}$, consistently with that shown by Faltinsen (1990). In terms of the expected largest values, the Rayleigh distribution underpredicts while the exponential distribution overpredicts them for both C_D values. The predictions by Stansberg's method agree well with the time-domain values, see the right two plots in the figure.

- Irregular waves with $H_s = 1$ m, $T_p = 5$ s:

  In this case, the ratio between the linearized eddy-making damping and the critical damping is $\xi = 6.48\%$ and 3.54%, respectively, when $C_D = 2.2$ and 0.9 are used. The exponential distribution and the Stansberg's method tend to overpredict the expected largest value while the Rayleigh distribution can well predict this value especially when the damping is small (i.e., $C_D = 0.9$ for which $\xi = 3.54\%$).

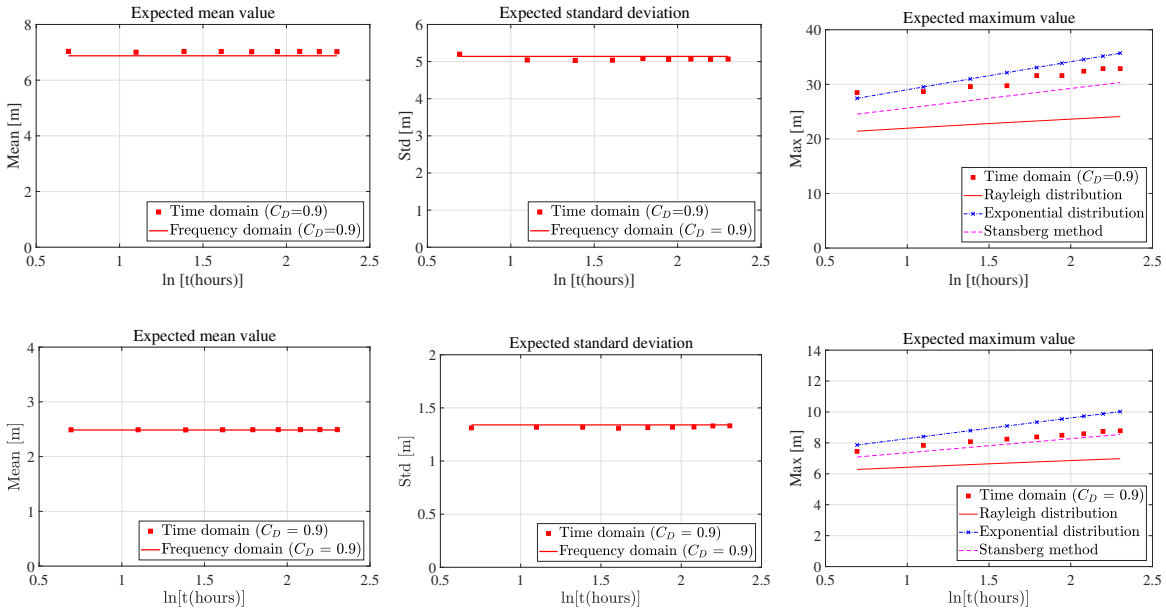

Figure 17: Expected mean value (left), standard deviation (middle) and maximum (right) value of the slow-drift sway motion of the well boat. Only the eddy-making damping is included. Upper: $H_s = 2$ m, $T_p = 6$ s, $U_\infty = 0.3$ m/s. Lower: $H_s = 1$ m, $T_p = 5$ s, $U_\infty = 0.3$ m/s. The predicted maximum value based on Rayleigh distribution, exponential distribution and Stansberg's method (Stansberg, 1991) are also shown.

The influence of current on the slow-drift motion is also examined. In particular, a current velocity $U_\infty = 0.3$ m/s leads to the results shown in Figure 17. The considered current velocity corresponds to a small to moderate current condition, see Table 1. As explained in section 3.2.6, the steady-flow drag coefficient should be used for cases in combined oscillatory flow and current when estimating the eddy-making damping. Therefore, a ship averaged drag coefficients $C_D = 0.9$ is adopted following the

analysis in steady current documented in Shen et al. (2018b). From the figure, the expected mean values and standard deviations from frequency domain match nicely with the time-domain results for both examined sea states. The eddy-making damping is linearized according to eq. (5) in the frequency-domain solution and the ratio between the equivalent linearized damping and the critical damping is $\xi = 13.86\%$ and 12.69% for case with $H_s = 2$ m and 1 m, respectively. Compared with the value without current, we can see that the presence of current significantly increases the ratio ξ, changing ξ from 8.89% to 13.86% for $H_s = 2$ m and $T_p = 6$ s and from 3.54% to 12.69% for $H_s = 1$ m and $T_p = 5$ s. When estimating the mean value of the sway motion in frequency domain, apart from the contribution from mean-wave load, the influence of current in connection with mean-drag force in sway should be also considered and written as

$$\frac{1}{T_N}\int_0^{T_N} B_D\left(\dot{\eta}_2^{(2)} - U_\infty\right)\left|\dot{\eta}_2^{(2)} - U_\infty\right| dt \approx \frac{1}{T_N}\int_0^{T_N} B_D\left[\dot{\eta}_{2a}^{(2)}\cos\left(\mu_N t\right) - U_\infty\right]\left|\dot{\eta}_{2a}^{(2)}\cos\left(\mu_N t\right) - U_\infty\right| dt \tag{13}$$

Here T_N is the damped natural period of the slow-drift motion considering linearized eddy-making damping, $\dot{\eta}_{2a}^{(2)} \approx \mu_n \sigma_{\eta_2^{(2)}}$ is the characteristic velocity amplitude of the slow-drift motion, $\mu_N = 2\pi/T_N$ and $\sigma_{\eta_2^{(2)}}$ are the corresponding natural wave frequency and standard deviation.

For the expected largest value, when current is present, the exponential distribution can provide an accurate prediction of this variable, especially for sea state with $H_s = 2$ m and $T_p = 6$ s.

4.1.3. Influence of the first-order motion on the slow-drift sway response

When evaluating the eddy-making damping, it is not common to account for the first-order velocity. However, this may matter for the slow-drift sway motion. To include the first-order velocity, we need to solve the first-order motion and slow-drift motion simultaneously. The motion equation eq. (1) is modified to account for the first-order motion and written as

$$\left[M + A_{22}\left(\infty\right)\right]\ddot{\eta}_2 + \int_0^t K_{22}\left(\tau\right)\dot{\eta}_2\left(t-\tau\right)d\tau + B_{22}^{SD}\dot{\eta}_2 + B_D\left(\dot{\eta}_2 - u_w - U_\infty\right)\left|\dot{\eta}_2 - u_w - U_\infty\right| + C_{22}\eta_2 = F_2 \tag{14}$$

Here η_2, $\dot{\eta}_2$ and F_2 are the motion, velocity and excitation force in sway, including both the first-order and slow-drift components. K_{22} is the retardation function and u_w is the transverse component of wave velocity, estimated at the position $0.5D$ below the center of gravity of the well boat, with D the mean draft of the well boat.

Time histories of the sway motion of the well boat without and with including the first-order motion are shown in Figure 18. For the slow-drift damping, only the eddy-making damping is considered, which means that B_{22}^{SD} in eq. (14) is set to zero. The figure shows that considering the first-order motion will reduce the maximum value of the slow-drift motion when $U_\infty = 0$ m/s (left plot), but will have a much smaller influence when $U_\infty = 0.3$ m/s (right plot). The presented results also show that the first-order motion is small compared with the slow-drift component for the considered sea states.

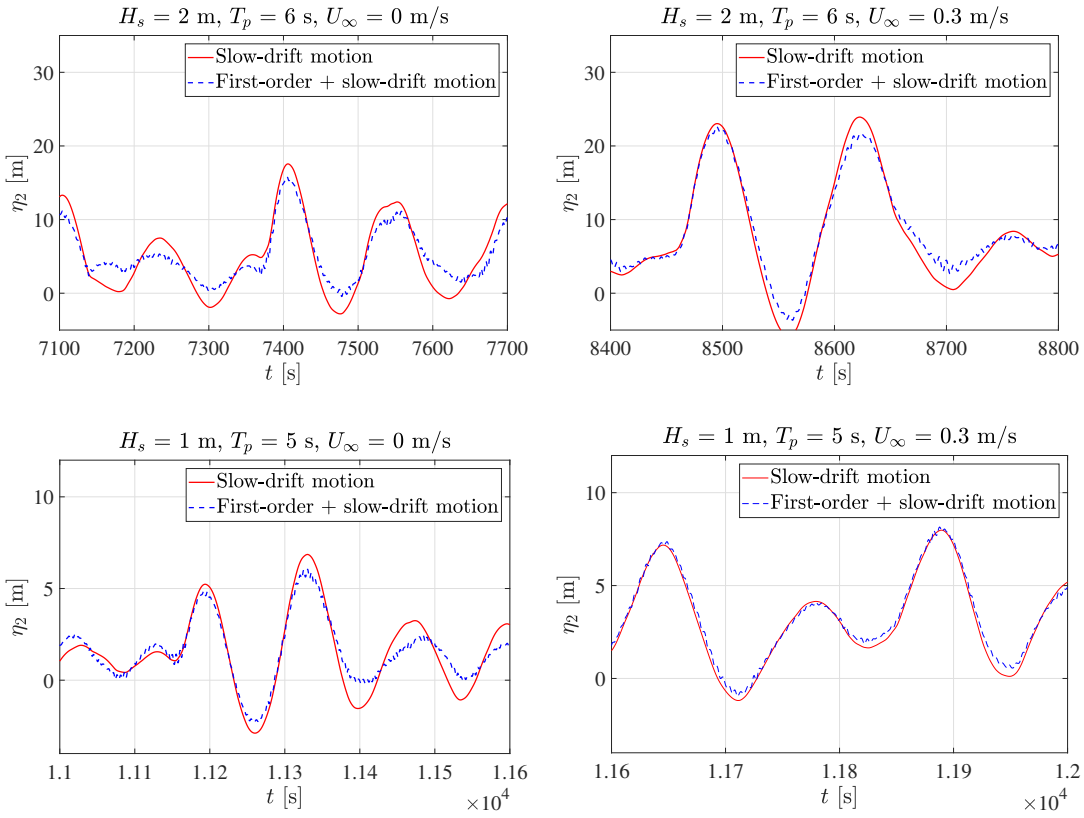

Figure 18: Time histories of the slow-drift sway motion of the well boat without and with considering the first-order motion. Upper: $H_s = 2$ m, $T_p = 6$ s. Lower: $H_s = 1$ m, $T_p = 5$ s. Left: irregular waves only ($U_\infty = 0$ m/s). Right: irregular waves and current ($U_\infty = 0.3$ m/s).

5. Dynamic response of the coupled well boat-fish farm system

In this section, we present a numerical investigation of the coupled well boat-fish farm system in irregular waves and current. The main purpose is to see how the presence of the well boat will influence the behavior of the fish farm and in this respect to determine the operational conditions of the well boat. The slow-drift sway motion of the well boat with a simplified mooring system has been studied and verified in section 4. The numerical model for the fish-farm system has been validated against experimental data in Shen et al. (2018a). This suggests that the numerical results of the coupled system can be reasonable and suitable for the analysis of well-boat operational limits in waves and current. Long-crested irregular waves and current in positive x_E direction (see Figure 1) are assumed. As shown in Shen et al. (2018b), the coupled system with set-up A (see Figure 3), with the well boat placed at the weather side of the floating collar is the most critical in terms of anchor-line loads and floating collar stresses, so this set-up is also our research focus. Results for the other set-up (set-up C) shown in Figure 3 will be considered in selected cases, for comparison. Nominal results are first shown in section 5.1. "Nominal" denotes that basis values and modelings are used in the simulations. The main attention is paid to the load in anchor line-1 (defined in Figure 1) and to the floating-collar stresses, which are two important parameters for the structural integrity of the fish farm. A sensitivity analysis is also performed in section 5.2 to identify important parameters affecting the maximum anchor loads and floating-collar stresses. Lastly, systematic simulations are

performed in section 5.3 to determine the operational conditions of the well boat.

5.1. *Nominal results*

In the nominal simulations, we try to model the coupled system as complete as possible. For the well boat, both the first-order motions and the slow-drift motions are included. The first-order motions are solved by the classical linear potential-flow theory, including all the six-degree-of-freedom motions. In terms of the slow-drift motions, the slow-drift surge, sway and yaw motions can be considered. For the coupled system with set-up A, the well boat is placed at the weather side of the fish farm, the slow-drift surge and yaw motions are expected to be small, therefore they are not considered in the simulations, i.e., only the slow-drift sway motion is included. Concerning the wave-drift damping, both the mean and the slowly-varying wave-drift damping are included. When formulating the eddy-making damping, both the first-order velocity and slow-drift velocity are accounted for. In terms of the fish farm, a realistic set-up (with single cage) is considered, including a floating collar, an elastic sinker tube, a flexible-closed net cage and a complex mooring system. The final motion equations of the well boat are similar to eq. (14), but for the six rigid degrees of freedom and the restoring provided by the fish farm is represented by contact and connect-line forces, as explained in Shen et al. (2018b).

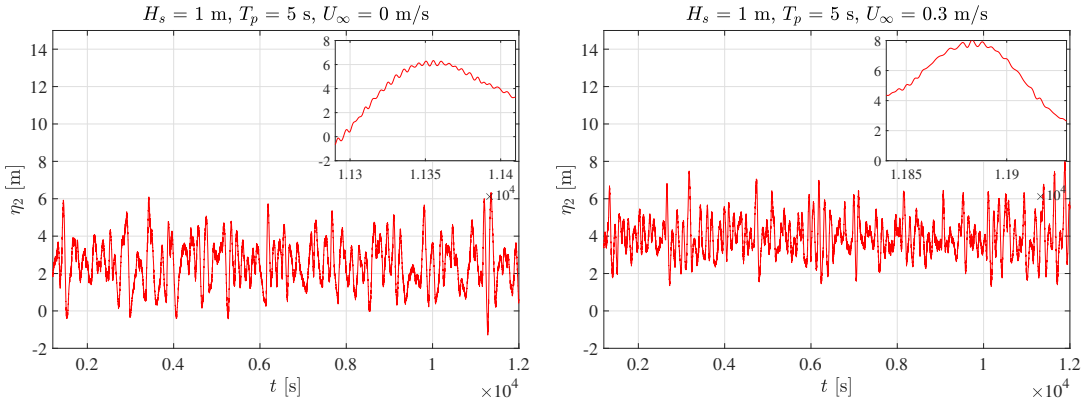

Figure 19: Time histories of the sway motion of the well boat when placed at the weather side of a fish farm (set-up A). A zoomed view is also given when the motion reaches the largest maximum within the examined simulated time (3 hours). Left: $H_s = 1$ m, $T_p = 5$ s and $U_\infty = 0$ m/s. Right: $H_s = 1$ m, $T_p = 5$ s and $U_\infty = 0.3$ m/s.

Time histories of the sway motion of the well boat in irregular waves and in combined irregular waves and current are shown, respectively in the left and right plot of Figure 19. The duration of the simulations is 3 hours. The considered environmental parameters are: significant wave height $H_s = 1$ m and peak period $T_p = 5$ s for the waves, and current velocity $U_\infty = 0$ m/s and 0.3 m/s. The ship averaged drag coefficients $C_D = 2.2$ and 0.9 are adopted, respectively, for $U_\infty = 0$ m/s and $U_\infty = 0.3$ m/s. From the figure, the presence of current increases the maximum sway motion from 6.33 m to 8.03 m, with an increment of about 26.4%. The figure also shows that the slow-drift motion dominates over the wave-frequency component for both cases, similarly to the results for the simplified system in Figure 18. The coupled system in sea state with $H_s = 2$ m and $T_p = 6$ s is also investigated and numerical results (not shown here) indicate that the maximum sway motion increases with similar magnitude due to the current. In particular, the increment is about 22%, with a change from 14.12 m to 17.23 m.

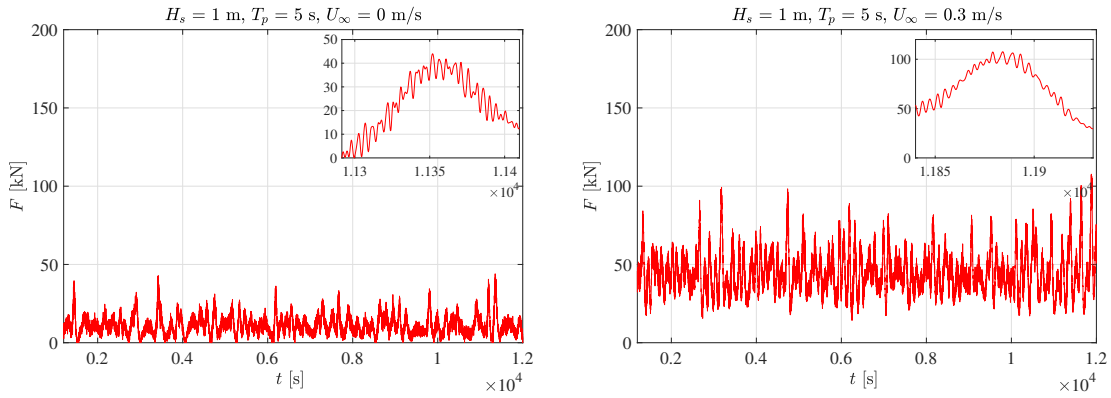

Figure 20: Same as in Figure 19, but for the loads in anchor line-1.

Figure 20 shows the time histories of the loads in anchor line-1 for the coupled system in sea state with $H_s = 1$ m and $T_p = 5$ s. From the figure, the wave-frequency component is small compared with the total anchor load, especially for the case with current. The time instant when the anchor load reaches the largest maximum coincides with that when the largest sway motion occurs within the examined simulated time (see Figure 19). The presence of current increases the maximum anchor load significantly, from 44 kN to 107.5 kN. There are two reasons: (1) the maximum sway motion of the well boat increases due to the current and (2) viscous loads on the net cage increase due to the current. Without the well boat, the maximum anchor loads are about 10 kN and 29 kN for $U_\infty = 0$ m/s and 0.3 m/s, respectively. It means that the well-boat presence increases the maximum anchor load by more than 300% both without and with current. When the coupled system is exposed to more severe sea states with $H_s = 2$ m and $T_p = 6$ s, the maximum anchor loads are 167 kN and 300 kN, respectively, for $U_\infty = 0$ m/s and 0.3 m/s. Without the well boat, much smaller maximum values are obtained, approximately 16.2 kN and 44 kN, respectively.

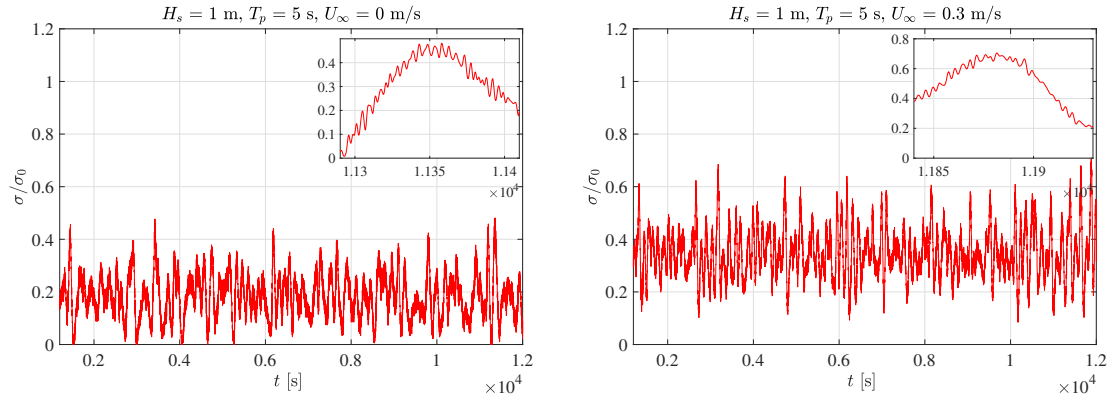

Figure 21: Same as in Figure 19, but for the stresses at $\beta = 180^o$ in the floating collar. The stress is made non-dimensional by the yield stress (high-density polyethylene).

Next, we show the results of the bending stresses in the floating collar due to its horizontal deformations. The way to estimate the stresses has been shown in Shen et al. (2018b). The maximum stress is expected to occur at $\beta = 180^o$ where the well boat is in contact with the floating collar (Shen et al., 2018b). Time histories of the stress at $\beta = 180^o$ in the floating collar are shown in Figure 21

for $H_s = 1$ m and $T_p = 5$ s. The largest maximum stress occurs at the time when the sway motion of the well boat reaches the largest maximum value within the examined simulated time. The maximum stresses are 0.48 σ_0 and 0.7 σ_0, respectively, for $U_\infty = 0$ m/s and 0.3 m/s. Here σ_0 is the yield stress (high-density polyethylene) for the floating collar. The obtained maximum stress for $U_\infty = 0.3$ m/s is close to the yield stress. This indicates that the examined sea conditions are of relevance when determining the operational conditions of the well boat.

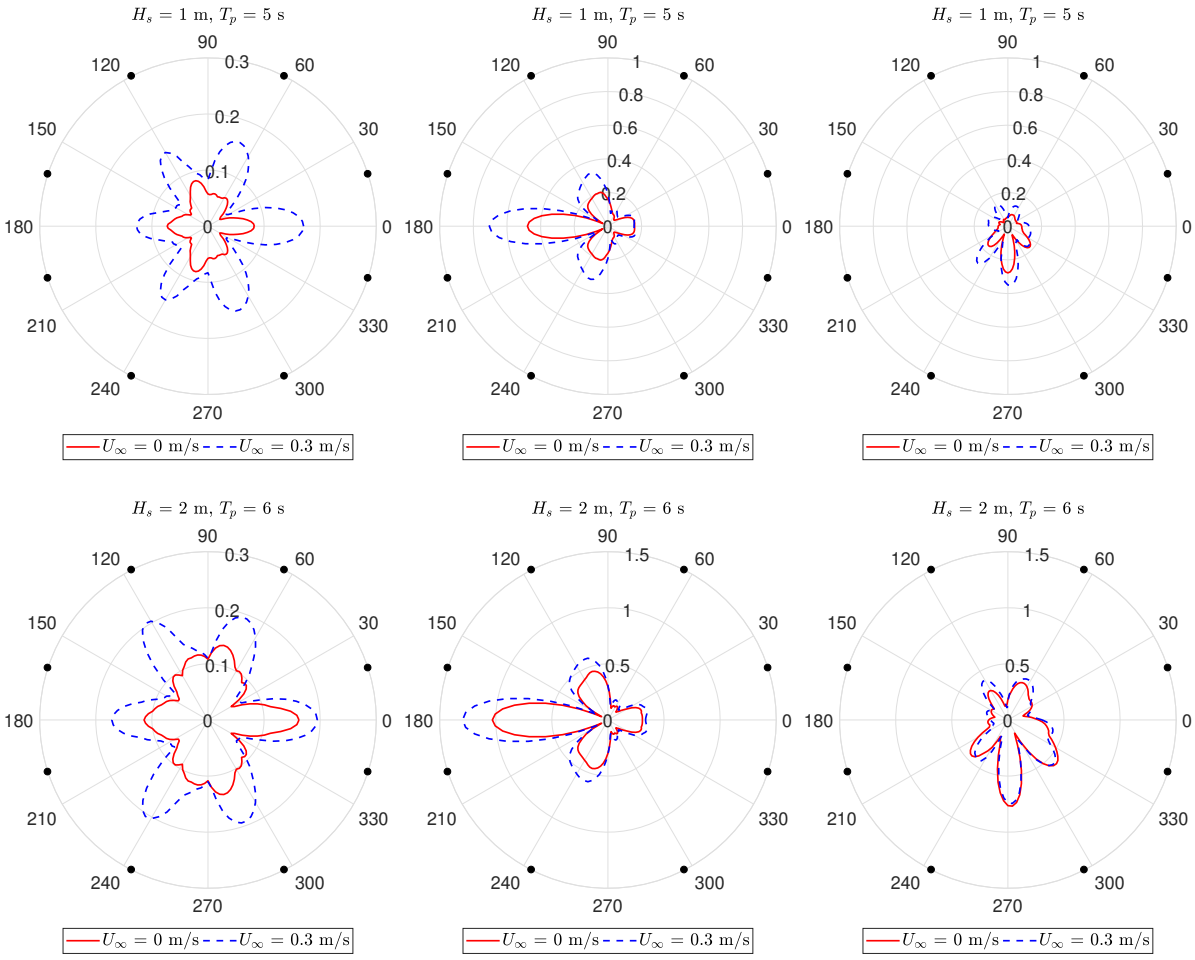

Figure 22: Maximum stress distribution along the floating collar due to horizontal deformations. The stress is made non-dimensional by the yield stress (high-density polyethylene). Left: fish-farm system only. Middle: coupled system with set-up A. Right: coupled system with set-up C. Upper: $H_s = 1$ m and $T_p = 5$ s. Lower: $H_s = 2$ m and $T_p = 6$ s. Solid lines: $U_\infty = 0$ m/s. Dashed lines: $U_\infty = 0.3$ m/s. The 8 solid circles in each plot represent the positions where bridle lines are attached to the floating collar.

To see more clearly how the well boat will influence the floating collar, the stress distribution along the floating collar due to horizontal deformations without and with the well boat are shown in Figure 22. Results for the coupled system with set-up C (see Figure 3) are also given for comparison. Two wave conditions with $H_s = 1$ m, $T_p = 5$ s and with $H_s = 2$ m, $T_p = 6$ s, respectively, are considered. Each wave condition is combined alternatively with two current velocities, $U_\infty = 0$ m/s and 0.3 m/s. From the figure, the presence of the well boat will change the stress distribution along the floating collar. For fish farm only, there are several peak values with similar amplitude along the floating collar, while for the coupled system, the maximum stress occurs at the region where the well boat is

in contact with the floating collar, respectively, at $\beta = 180^o$ for set-up A and at $\beta = 270^o$ for set-up C. For cases with $H_s = 1$ m and $T_p = 5$ s, without the well boat, the maximum stresses are about 0.08 σ_0 and 0.17 σ_0, respectively, for $U_\infty = 0$ m/s and 0.3 m/s while for the coupled system, with set-up A the corresponding values are 0.48 σ_0 and 0.7 σ_0 and with set-up C the corresponding values are 0.27 σ_0 and 0.35 σ_0. The results show that the maximum stresses increase significantly due to the well boat and the coupled system with set-up A is more critical, as expected.

For cases with $H_s = 2$ m and $T_p = 6$ s without the well boat, the maximum stresses are about 0.162 σ_0 and 0.195 σ_0 for $U_\infty = 0$ m/s and 0.3 m/s, respectively, while for set-up A the corresponding values are 1.03 σ_0 and 1.3 σ_0 and for set-up C the corresponding values are 0.74 σ_0 and 0.76 σ_0. The results show that the maximum stress for the coupled system with set-up A will exceed the yield stress for the considered H_s sea state even without current. One should note that, for the coupled system with set-up C, the well boat will have a pendulum motion relative to the floating collar, see Figure 23. If one more rope is used to connect the well boat and the floating collar, inserted between the two existing ropes and with connecting position at the floating collar $\beta = 270^o$, a significant reduction ($\approx 30\% - 40\%$) of the maximum stress with respect to the original value is observed.

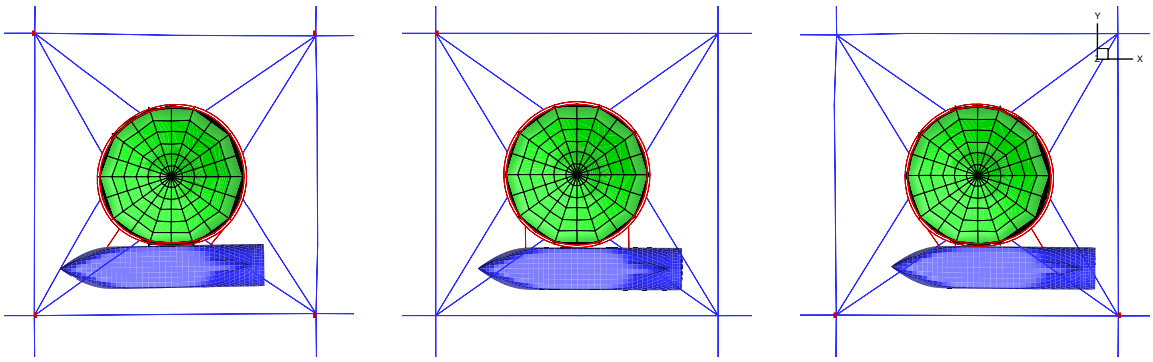

Figure 23: Sketch for the coupled system with set-up C in three different time instants showing the pendulum motion of the well boat relative to the floating collar.

5.2. Sensitivity analysis

Due to uncertainties in the mathematical modeling and system set-up, we performed a sensitivity analysis for the coupled system in irregular waves and current. The main focus is on the maximum loads in anchor line-1 (defined in Figure 1) and the maximum stresses in the floating collar. The inflow is in the positive x_E direction ($\alpha_c = 0^o$, $\alpha_w = 0^o$). The well boat is assumed to be placed at the weather side of the fish farm (set-up A). For the irregular waves, $H_s = 1$ m and $T_p = 5$ s, are considered, combined with two current conditions, i.e., $U_\infty = 0$ m/s and 0.3 m/s. The different parameters examined are shown in Table 2. In order to quantify their significance and try to identify the critical ones, we present condensed results in Figure 24 for the maximum load in anchor line-1 and in Figure 25 for the maximum stress in the floating collar. Each bar represents the percentage difference with respect to the corresponding nominal value (documented in section 5.1). More detailed discussions are presented in section 5.2.1 for the anchor loads and in section 5.2.2 for the floating collar stresses.

Table 2: Parameters varied in the sensitivity analysis for cases in irregular waves and current. $C_{D,0}$ and $k_s, 0$ are, respectively, the ship averaged drag coefficient and anchor-line stiffness used in the nominal simulations. $C_{D,0} = 2.2$ and 0.9 for cases without and with current, respectively. N_h and N_v are the number of structural modes used for the floating collar, respectively, in horizontal and vertical directions and $N_h = 7$ and $N_v = 8$ are found from convergence studies and used in the nominal simulations. The nominal value of the pretension force in the anchor line is 10 kN.

	No.	Value	Explanation
Wellboat	1	$C_D = 1.2C_{D,0}$	Drag coefficient
	2	$C_D = 0.8C_{D,0}$	Drag coefficient
	3	$\bar{B}_{22}^{SD}$	Wave-drift damping
	4	$\eta_2^{(2)} + \eta_2^{(1)}$	First-order + slow-drift motion, cage neglected
	5	$\eta_2^{(2)}$	Slow-drift motion, with cage
	6	$\eta_2^{(2)}$	Slow-drift motion, cage neglected
Floating collar	7	N_h=3, N_v=4	Less modes
Moorings	8	Pretension = 5 kN	Pretension
	9	Pretension = 15 kN	Pretension
	10	$k_s = 2.0k_{s,0}$	Anchor line stiffness

5.2.1. Loads in anchor line-1

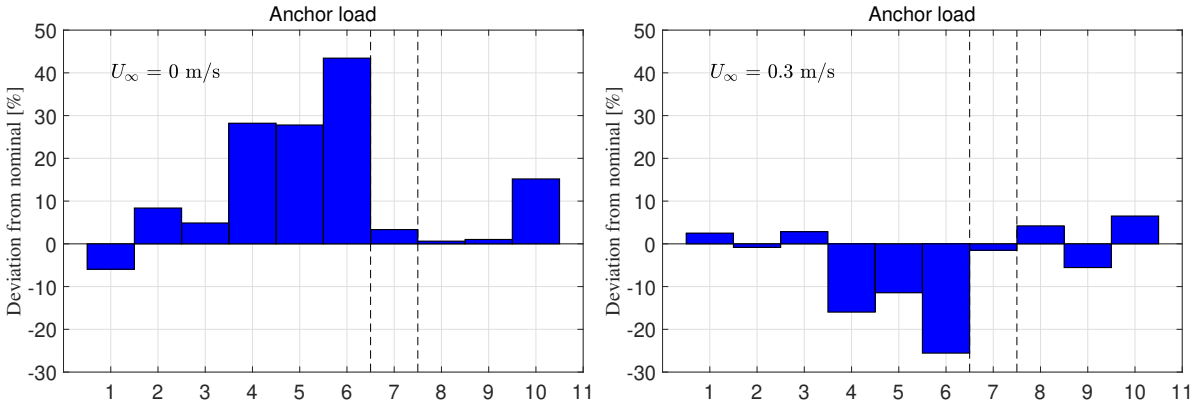

Figure 24: Each bar represents the percentage difference of the anchor load (maximum value) with respect to the nominal value. The considered H_s= 1 m and T_p = 5 s. The numbers on the horizontal axis refer to the variation number as given in Table 2. Left: U_∞ = 0 m/s. Right: U_∞ = 0.3 m/s.

Well boat: The maximum anchor load is closely connected with the slow-drift sway motion of the well boat, so the main attention in the sensitivity analysis is paid to parameters that may be important for the slow-drift motion.

First we examine the influence of the ship averaged drag coefficient. The cross-sectional drag coefficients C_D for the well boat are estimated empirically and assumed KC-number independent in the nominal simulations. In reality, C_D may slightly vary with KC for small KC number. Furthermore, the influence of first order motions on C_D is not considered. So an error in the boat drag coefficient is expected. Changing the ship averaged drag coefficient by 20% will lead to about 6%-8% change of the maximum anchor load with respect to the nominal value when U_∞ = 0 m/s. Negligible influence is observed for the case with current.

For the wave-drift damping, considering the mean wave-drift damping instead of the time-varying wave-drift damping will increase the maximum anchor load, by about 5% and 3%, respectively, for cases without and with current.

Next, we want to quantify how the maximum anchor load will be influenced when simplified modeling of the coupled system is adopted. The main purpose of simplifying the modeling is to increase the computational efficiency. In the nominal simulations, for sea state with $H_s = 1$ m and $T_p = 5$ s, a time step in the range of 0.03 s is needed to reach convergence and it takes about 4.8-5 hours computational time on a 2.8 GHZ one-core laptop for a simulated time $t_s = 3$ hours. For more severe sea states, smaller time step is needed and greater computational time is expected. Although the developed numerical solver is efficient enough compared with available commercial softwares, it is still interesting to see whether it is possible to increase the computational efficiency by simplifying the numerical modeling, while still preserving reasonable accuracy. In the following analysis, in terms of the wave-drift damping, only the mean wave-drift damping is considered in the simulations.

Net cage: Modeling the net cage is challenging in the simulations and the latter may more easily break down with the presence of net cage due to the occurrence of unphysical negative tensions, especially in irregular waves with higher H_s. Neglecting the net cage, i.e., modeling the fish-farm effect only in terms of the mooring lines and the floating collar, will increase the maximum anchor load by about 28% when $U_\infty = 0$ m/s, but will reduce the value by about 15.9% when $U_\infty = 0.3$ m/s. The maximum sway motion of the well boat will increase if the net cage is neglected, this will tend to increase the maximum anchor load, but neglecting the net cage means that the loads on the net cage are not included, this will tend to reduce the maximum anchor load. So the actual change of the maximum anchor load with respect to its nominal value depends on the joint effects of these two factors. The fact that the maximum anchor load increases without current will then mean that in this case the increase of sway motion dominates with respect to the net-cage loads not included, while the opposite occurs in current. Neglecting the net cage will reduce the computational time by about 20%.

First-order motion: To predict the first-order motions of the well boat, transient effects are included in the motion equations. This is time consuming. Neglecting the first-order response, i.e., only considering the slow-drift motions for the well boat and the fish farm, will increase the maximum anchor load by about 28 % when $U_\infty = 0$ m/s, but will reduce the value by about 11.5% when $U_\infty = 0.3$ m/s. The computational time will be reduced by about 50% when only the slow-drift motions are considered.

First-order motion + net cage: If both the first-order motion and the net cage are neglected, the maximum anchor load will increase by about 43% when $U_\infty = 0$ m/s but will reduce by about 26% when $U_\infty = 0.3$ m/s. The computational time will be reduced by about 90%.

Selected fish-farm related parameters are also examined and detailed results are given in the following.

Floating collar: The influence of the number of modes used for the floating collar is studied and numerical results indicate that modeling the floating collar with less modes in both the lateral and

vertical directions will have small influence on the maximum anchor load.

Mooring system: In the nominal simulations, the pretension force in the anchor line is 10 kN. Increasing the pretension force by 50% or reducing the value by 50% will lead to a moderate influence on the maximum anchor load. Increasing the stiffness of anchor lines by 100% will increase the maximum anchor load by 15% when $U_\infty = 0$ and a smaller increment, i.e., about 6.5%, is observed when $U_\infty = 0.3$ m/s.

5.2.2. Maximum stress in the floating collar

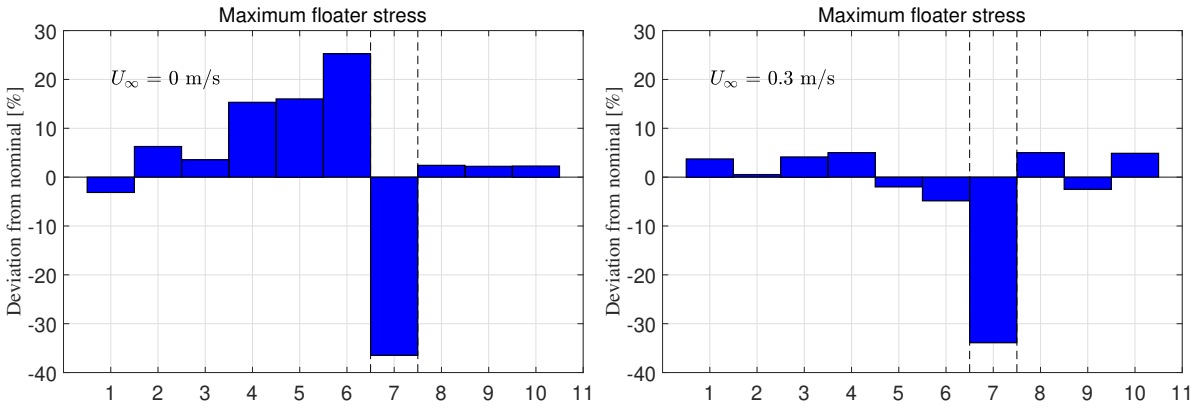

Figure 25: Same as in Figure 24, but for the maximum stress in the floating collar at the position $\beta = 180^o$.

The sensitivity of the maximum stress to the different parameters is similar to that of the maximum anchor load when $U_\infty = 0$ m/s, but when $U_\infty = 0.3$ m/s the maximum stress is not sensitive to the majority of the examined parameters, with a maximum variation of about 5% with respect to the nominal value. The only exception is No.7, when less modes are used to model the floating collar. In nominal simulations, $N_h = 7$ and $N_v = 8$ are found sufficient for convergence purpose. If less modes are used with $N_h = 3$ and $N_v = 4$, a significant reduction of the maximum stress, about 35%, is observed. It implies that the elasticity of the floating collar must be properly modeled to have a reliable prediction of the maximum floating-collar stress.

5.3. Operational conditions

In this section, we will discuss how to determine the operational conditions of the well boat when at the fish farm for the loading/offloading operation. The well boat is moored at the weather side of the fish farm. As explained in Shen et al. (2018b), two operational criteria are proposed connected, respectively, with maximum forces in the mooring lines and maximum stresses in the floating collar. In the present work, we mainly focus on the coupled well boat-fish farm system in irregular waves and current. The simulation matrix is shown in Table 3, covering the scenario from small exposure to high exposure, according to the Norwegian Standard (see Table 1). For sea states with $H_s = 2$ m, only irregular waves are considered ($U_\infty = 0$ m/s). The ship averaged drag coefficient $C_D = 2.2$ and 0.9 are adopted, respectively, for $U_\infty = 0$ m/s and $U_\infty > 0$ m/s. The duration of each simulation is 3 hours.

Table 3: Environmental matrix used in the simulations for determining the operational conditions, showing current velocity U_∞ and significant wave height H_s, respectively, in the first column and first row. Four current velocities and three significant wave heights are considered. The remaining cells give the examined peak-period T_p ranges. For each examined T_p range, an interval $\Delta T_p = 1$ s is used.

Current U_∞ [m/s]	H_s [m]		
	0.5	1	2
0.0	2-3 s	2-5 s	3-6 s
0.1	2-3 s	2-5 s	-
0.3	2-3 s	2-5 s	-
0.5	2-3 s	2-5 s	-

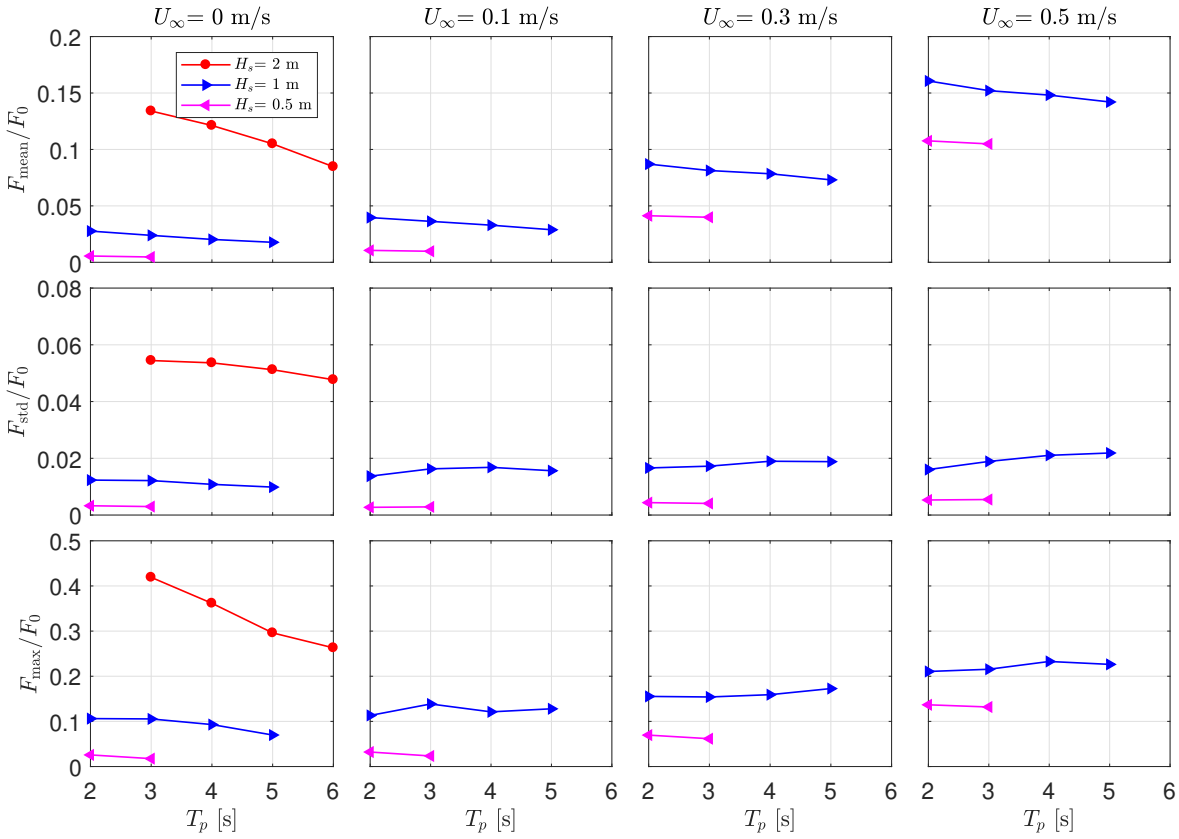

Figure 26: Mean value (upper row), standard deviation (middle row) and maximum value (lower row) of the force in anchor line-1. The force is made non-dimensional by the minimum breaking force F_0, which is 628 kN for polysteel rope with 3 strands and a diameter 64 mm. From left to right: current velocities $U_\infty = 0$ m/s, 0.1 m/s, 0.3 m/s, 0.5 m/s.

Numerical results of the force in anchor line-1 are given in Figure 26. Mean value, standard deviation and maximum value are provided. The maximum force experienced by the anchor line for the considered sea states is about $0.42F_0$ with $F_0 = 628$ kN the minimum breaking force for the considered anchor polysteel rope. The maximum anchor load for the considered sea states is less than 50% of the breaking limit, so it should not be of concern. For a given H_s without current, all the three examined parameters decrease with increasing peak period T_p. For a given H_s with current, the mean anchor load decreases while the standard deviation and maximum value of the anchor load tend to increase with increasing T_p. For a given T_p and H_s, the maximum anchor load tends to increase

with increasing U_∞.

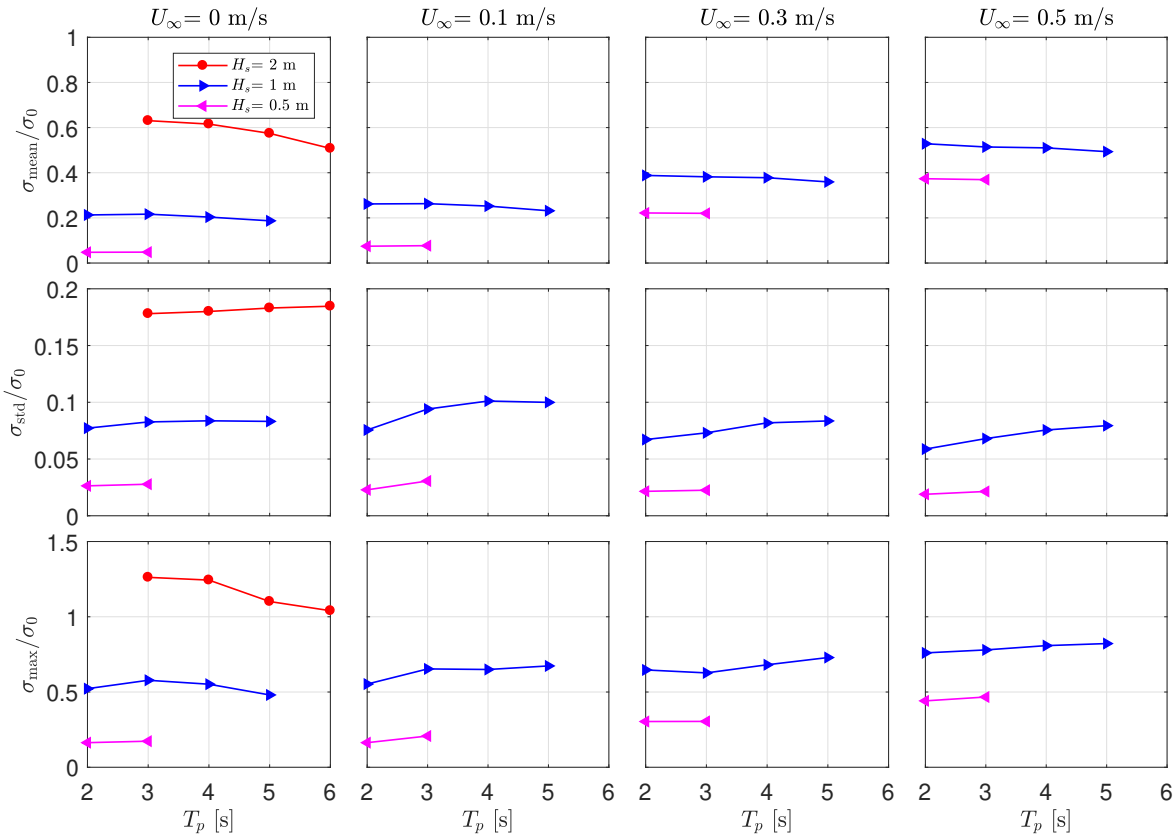

Figure 27: Same as in Figure 26, but for the stress in the floating collar at position $\beta = 180^{\mathrm{o}}$. The stress is made non-dimensional by the yield stress (high-density polyethylene).

Finally, we show the numerical predictions of the maximum stress in the floating collar due to its horizontal deformations. The results for cases in current only (Shen et al., 2018b) showed that the maximum stress due to horizontal deformations occurs at the position $\beta = 180^{\mathrm{o}}$ (defined in Figure 1) where the well boat is in contact with the floating collar. In Figure 27, we present the predicted maximum stresses at the position $\beta = 180^{\mathrm{o}}$. From the figure, the maximum stress is influenced by the different environmental parameters in a similar way as for the maximum anchor load. For a given H_s without current, the maximum stress tends to decrease with increasing T_p, especially for higher H_s, while an opposite trend is observed in current. For given H_s and T_p, a higher current velocity will lead to larger maximum stress. The maximum stress will exceed the yield stress for sea states with H_s = 2 m. For cases with H_s = 1 m, the maximum stress predicted for the examined sea states is about $0.82\sigma_0$ with σ_0 the yield stress of the floating collar. This indicates that H_s = 1 m is relevant for determining the operational conditions of the well boat. It should be noted that just one realization is considered in the analysis and actual results in irregular waves are realization dependent for the considered simulated time, nevertheless they can still provide a valuable guidance for determining the operational conditions of the well boat. Also, we just examine the coupled system in the most critical scenario with long-crested irregular waves and current aligned. The coupled system in more general sea states should also be studied and possibly three-dimensional waves should be accounted for. This is left for future investigations.

6. Conclusions

A numerical study of a well boat operating at a fish farm in irregular long-crested waves and current was performed. The main target was to assess the influence of the well-boat presence on the fish farm and in this respect to determine the operational conditions of the well boat. A modern design well boat and a realistic fish farm were considered in the analysis. Both the well boat and the fish farm were modeled with state-of-the-art theoretical and numerical formulations. For instance, a structural truss model was combined with a hydrodynamic screen model and Løland's wake model to describe the net cage behavior in a time efficient way. The latter is crucial in investigating the behavior in irregular sea. The method is accurate and robust except if negative twine tensions occur in larger sea states.

The slow-drift sway motion of the well boat was investigated at first by simplifying the influence of the net cage in terms of a restoring term. Hydrodynamic and statistical theories of the motion were presented. Numerical results indicated that both the mean and the slowly-varying wave-drift damping are important, especially for cases with larger significant wave height. When estimating the eddy-making damping, both first-order and slow-drift velocities should be included. The results also showed that Rayleigh distribution can be used to predict the extreme values when the damping is small (i.e., linearized damping $<$ 3-4% of the critical damping). For cases in combined irregular waves and current, exponential distribution is more suitable to predict the extreme values. The simplified analysis involved an analytically-oriented approach and served as a verification of the complete time-domain analysis of the coupled well boat-fish farm system. An empirical method was proposed to determined drag coefficients for the ship. Important parameters are section geometry, Keulegan-Carpenter number, three-dimensional flow at the ship ends, and in addition, Reynolds number and reduced velocity with the presence of current. The procedure was validated by comparing with published free-decay model tests in sway of a moored ship.

A physical investigation of a coupled well boat-fish farm system was also performed, with the well boat moored at the weather side of the fish farm. Detailed analysis of the maximum load in one of the front anchor lines and of the maximum stress in the floating collar was given. Numerical results showed that both of them increase significantly due to the well boat. The increment can be more than 300% when the system operates in moderate exposure sea states.

A sensitivity analysis was also performed to identify important factors influencing the maximum load in anchor line-1 and the maximum stress in the floating collar. The study showed that the examined two variables were in general more sensitive to the variation of different parameters for cases without current than with current. The cross-sectional drag coefficients for the well boat and the fish-farm related parameters, like the pretension load in the anchor lines and anchor-line stiffness, have moderate influence on the two variables. Sufficient number of structural modes for the floating collar should be used for a reliable prediction of the maximum floating-collar stress. Simplifying the modeling of the coupled system, for instance, neglecting the net cage and the first-order motion has more effect on the maximum anchor load than on the maximum floating-collar stress and smaller influence on the maximum floating-collar stress was observed when current is present.

Lastly, the operational conditions of the well boat were investigated through systematic simulations. Two criteria were examined based on the limit for the maximum loads in the mooring lines and for the maximum stress in the floating collar, respectively. Numerical results showed that the maximum anchor load will not exceed the anchor-line breaking limit even in high exposure sea conditions and thus it should not be of concern. The maximum stress in the floating collar would be close to the yield stress when the system operates in moderate exposure sea states, and should be used to determine the operational conditions of the well boat. The conclusions are similar to those in current only, previously examined (Shen et al., 2018b). However, in the same current condition, the presence of irregular waves would significantly increase, for instance, the maximum floating-collar stress, due to the slow-drift motion of the well boat.

Although we studied a typical floating-collar fish farm, the numerical solver proposed in this paper is applicable to any net-based fish farm concept and can also be used to analyze the operational condition of novel fish-farm designs, supported by conventional offshore platforms. The effect of short-crested sea as well as the presence of several near-by fish cages should be investigated in the future. Furthermore, the approaching and leaving phases of the well boat need to be studied. The presence of fish inside the net cage matters (see He et al., 2018) and represents an uncertainty in our analysis.

Acknowledgement

This work was supported by the Research Council of Norway through the Centers of Excellence funding scheme AMOS, project number 223254. Rolls-Royce Marine is acknowledged for providing the geometry information of the well boat.

References

Abramowitz, M., Stegun, I. A., 1965. Handbook of mathematical functions: with formulas, graphs, and mathematical tables. Vol. 55. Courier Corporation.

Aranha, J., 1994. A formula for 'wave damping'in the drift of a floating body. Journal of Fluid Mechanics 275, 147–155.

Bearman, P. W., Graham, J. M. R., Obasaju, E. D., Drossopoulos, G. M., 1984. The influence of corner radius on the forces experienced by cylindrical bluff bodies in oscillatory flow. Applied Ocean Research 6 (2), 83–89.

BureauVeritas, 2016. Hydrostar for experts user manual. Research Department of Bureau Veritas.

Faltinsen, O. M., 1990. Sea loads on ships and ocean structures. Cambridge University Press, Cambridge, England.

Faltinsen, O. M., Dahle, L. A., Sortland, B., 1986. Slowdrift amping and response of a moored ship in irregular waves. In: Proceedings of the Fifth International Symposium on Offshore Mechanics and Arctic Engineering. American Society of Mechanical Engineers, pp. 297–303.

Faltinsen, O. M., Minsaas, K. J., Liapis, N., Skjørdal, S. O., 1980. Prediction of resistance and propulsion of a ship in a seaway. In: Proceedings of the 13th symposium on naval hydrodynamics, Tokyo, Japan. pp. 505–229.

Faltinsen, O. M., Sortland, B., 1987. Slow drift eddy making damping of a ship. Applied ocean research 9 (1), 37–46.

Faltinsen, O. M., Timokha, A. N., 2009. Sloshing. Cambridge university Press, Cambridge, England.

Faltinsen, O. M., Zhao, R., 1989. Slow-drift motions of moored two-dimensional body in irregular waves. Journal of ship research 33 (2), 93–106.

Hamel-Derouich, D., 1993. Hydrodynamic forces on rectangular cylinders horizontally submerged in waves and currents at low kc numbers. In: The Third International Offshore and Polar Engineering Conference. International Society of Offshore and Polar Engineers, pp. 168–175.

He, Z., Faltinsen, O. M., Fredheim, A., Kristiansen, T., 2018. The influence of fish on the mooring loads of a floating net cage. Journal of Fluids and Structures 76, 384–395.

Jonsson, I. G., 1980. A new approach to oscillatory rough turbulent boundary layers. Ocean Engineering 7 (1), 109 – 152.

Naess, A., 1986. The statistical distribution of second-order slowly-varying forces and motions. Applied Ocean Research 8 (2), 110–118.

Naess, A., 1989. Effects of correlation on extreme slow-drift response. In: Proc 8th Int Offshore Mechanics and Arctic Engineering Symposium, Hague, Netherlands. Vol. 2. pp. 465–474.

NS9415, 2009. Marine fish farms - requirements for site survey risk, analysis, design, dimensioning, production,installation and operation. Norwegian standard.

Price, W. G., Bishop, R. E. D., 1974. Probabilistic theory of ship dynamics. Chapman and Hall, London, England.

Roberts, J. B., Spanos, P. D., 2003. Random vibration and statistical linearization. Dover Publications, New York, USA.

Sarpkaya, T., Storm, M., 1985. In-line force on a cylinder translating in oscillatory flow. Applied Ocean Research 7 (4), 188–196.

Shen, Y., Greco, M., Faltinsen, O. M., Nygaard, I., 2018a. Numerical and experimental investigations on mooring loads of a marine fish farm in waves and current. Journal of Fluids and Structures 79, 115–136.

Shen, Y. G., Greco, M., Faltinsen, O. M., 2016. Numerical study of a coupled well boat-fish farm system in waves and current during loading operations. In: The 12th International Conference on Hydrodynamics (ICHD 2016), Egmond aan Zee, The Netherlands. Online proceedings, document No.98.

Shen, Y. G., Greco, M., Faltinsen, O. M., 2018b. Numerical study of a well boat operating at a fish farm in current. Journal of Fluids and Structures, submitted.

Stansberg, C. T., 1991. A simple method for estimation of extreme values of non-gaussian slow-drift responses. In: The First International Offshore and Polar Engineering Conference. International Society of Offshore and Polar Engineers, pp. 442–451.

Tanaka, N., Ikeda, Y., Nishino, K., 1982. Hydrodynamic viscous force acting on oscillating cylinders with various shapes. In: Proceedings of 6th Symposium on Marine Technology, Society of Naval Architecture of Japan.

Zhao, R., Faltinsen, O. M., 1988. Interaction between waves and current on a two-dimensional body in the free surface. Applied Ocean Research 10 (2), 87–99.